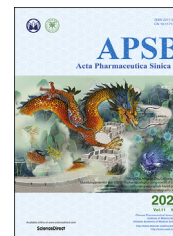




Chinese Pharmaceutical Association
Institute of Materia Medica, Chinese Academy of Medical Sciences

Acta Pharmaceutica Sinica B

www.elsevier.com/locate/apSB
www.sciencedirect.com



ORIGINAL ARTICLE

Discovery of thiosemicarbazone derivatives as effective New Delhi metallo- β -lactamase-1 (NDM-1) inhibitors against NDM-1 producing clinical isolates



Bing Zhao^{a,†}, Xinhui Zhang^{a,†}, Tingting Yu^a, Ying Liu^a,
Xiaoling Zhang^a, Yongfang Yao^a, Xuejian Feng^a, Hongmin Liu^a,
Dequan Yu^{b,*}, Liying Ma^{a,*}, Shangshang Qin^{a,*}

^aState Key Laboratory of Esophageal Cancer Prevention and Treatment, Key Laboratory of Technology of Drug Preparation (Zhengzhou University), Ministry of Education of China, Key Laboratory of Henan Province for Drug Quality and Evaluation, Institute of Pharmaceutical Research and School of Pharmaceutical Sciences, Zhengzhou University, Zhengzhou 450001, China

^bState Key Laboratory of Bioactive Substance and Function of Natural Medicines, Institute of Materia Medica, Chinese Academy of Medical Sciences and Peking Union Medical College, Beijing 100050, China

Received 28 March 2020; received in revised form 2 June 2020; accepted 28 June 2020

KEY WORDS

Thiosemicarbazone derivatives;
New Delhi metallo- β -

Abstract New Delhi metallo- β -lactamase-1 (NDM-1) is capable of hydrolyzing nearly all β -lactam antibiotics, posing an emerging threat to public health. There are currently less effective treatment options for treating NDM-1 positive “superbug”, and no promising NDM-1 inhibitors were used in clinical practice. In this study, structure–activity relationship based on thiosemicarbazone derivatives was

Abbreviations: 3-AP, 3-aminopyridine carboxaldehyde thiosemicarbazone; AcOH, acetic acid; Boc, *tert*-butoxycarbonyl; (Boc)₂O, di-*tert*-butyl decarbonate; CLSI, Clinical and Laboratory Standards Institute; conc. HCl, concentrated hydrochloric acid; DMAP, 4-dimethylaminopyridine; DpC, di-2-pyridylketone-4-cyclohexyl-4-methyl-3-thiosemicarbazone; *E. coli*, *Escherichia coli*; EDTA, ethylene diamine tetraacetic acid; ESI, electrospray ionization; HR-MS, high-resolution mass spectra; IC₅₀, half-maximal inhibitory concentrations; *K. pneumoniae*, *Klebsiella pneumoniae*; LQTS, long QT syndrome; MBLs, metallo- β -lactamases class B; MEM, meropenem; MHA, Mueller-Hinton Agar; MHB, Mueller-Hinton Broth; MIC, minimum inhibitory concentration; NDM-1, New Delhi metallo- β -lactamase-1; PBS, phosphate-buffered saline; PK, pharmacokinetic; RBCs, red blood cells; r.t., room temperature; SAR, structure–activity relationship; THF, tetrahydrofuran; TLC, thin layer chromatography; TMS, tetramethylsilane; UPLC, ultra-performance liquid chromatography.

*Corresponding authors. Tel./fax: +86 371 67781908.

E-mail addresses: dqyu@imm.ac.cn (Dequan Yu), maliying@zzu.edu.cn (Liyong Ma), qinss@zzu.edu.cn (Shangshang Qin).

[†]These authors made equal contributions to this work.

Peer review under responsibility of Institute of Materia Medica, Chinese Academy of Medical Sciences and Chinese Pharmaceutical Association.

<https://doi.org/10.1016/j.apSB.2020.07.005>

2211-3835 © 2021 Chinese Pharmaceutical Association and Institute of Materia Medica, Chinese Academy of Medical Sciences. Production and hosting by Elsevier B.V. This is an open access article under the CC BY-NC-ND license (<http://creativecommons.org/licenses/by-nc-nd/4.0/>).

lactamase-1;
Inhibitor;
Antibiotic resistance

systematically characterized and their potential activities combined with meropenem (MEM) were evaluated. Compounds **19bg** and **19bh** exhibited excellent activity against 10 NDM-positive isolate clinical isolates in reversing MEM resistance. Further studies demonstrated compounds **19bg** and **19bh** were uncompetitive NDM-1 inhibitors with $K_i = 0.63$ and $0.44 \mu\text{mol/L}$, respectively. Molecular docking speculated that compounds **19bg** and **19bh** were most likely to bind in the allosteric pocket which would affect the catalytic effect of NDM-1 on the substrate meropenem. Toxicity evaluation experiment showed that no hemolysis activities even at concentrations of 1000 mg/mL against red blood cells. *In vivo* experimental results showed combination of MEM and compound **19bh** was markedly effective in treating infections caused by NDM-1 positive strain and prolonging the survival time of sepsis mice. Our finding showed that compound **19bh** might be a promising lead in developing new inhibitor to treat NDM-1 producing superbug.

© 2021 Chinese Pharmaceutical Association and Institute of Materia Medica, Chinese Academy of Medical Sciences. Production and hosting by Elsevier B.V. This is an open access article under the CC BY-NC-ND license (<http://creativecommons.org/licenses/by-nc-nd/4.0/>).

1. Introduction

The discovery and development of antibiotics was considered one of the greatest breakthroughs in the 20th century¹. However, the emergence of multi-drug and even extensively drug-resistant pathogens due to the abuse or overuse of antibiotics in both clinical practice and farm animal production, posed an emerging threat to the treatment of bacterial infection². As a member of the main antibiotics, β -lactams agents were widely used in the clinic. Unfortunately, the clinical value of β -lactams has been challenged by the emergence and dissemination of β -lactamases which were able to destroy β -lactams by hydrolysis of the β -lactam ring. The β -lactamases can be grouped into four classes according to the Ambler classification scheme, the serine residue dependent class A, C, D, and the metallo- β -lactamases class B (MBLs)^{3–6}. MBLs are zinc-dependent and can be classified into three subunits, B1, B2 and B3, according to the number of zinc atoms in the active site^{2,7}. New Delhi metallo- β -lactamase-1 (NDM-1) which belongs to the subclass B1, was first discovered in 2008⁸ and was demonstrated with the capability of hydrolyzing nearly all β -lactam antibiotics except monobactams⁹. NDM-1 has experienced the fastest and widest geographical spread among MBLs, and bacterial infections harbouring plasmid-encoded NDM-1 have rapidly emerged worldwide^{10,11}, thus are the most troublesome.

Therefore, there is a strong demand to develop effective inhibitors of NDM-1 to tackle this bacterial resistance.

The majority of reported inhibitors of NDM-1 were non-covalent inhibitors¹², including chelating agents and zinc coordinating agents, such as compounds **1–4**^{13–16} (Fig. 1). Compounds **1** (AMA) and **2** could chelate zinc ions of protein to inhibit the activity of NDM-1. Compound **1** was an inhibitor of NDM-1 and other MBLs as well, whereas it was completely ineffective against the metallo- β -lactamases class A, C and D¹⁶. Compounds **3** and **4** (methisazone) were zinc coordinating inhibitors, molecules able to coordinate the zinc ions within the NDM-1 binding site^{13,15}. Although some effective molecules have been reported, concurrently, there are neither clinical drugs which can reverse the resistance mediated by NDM-1 nor approved NDM-1 inhibitors which are in clinical trials. Additionally, the variability of the loop arrangement at the active site as well as the rapidly evolved nature of NDM-1 variants made the development of efficient inhibitors more problematic^{17–20}.

Thiosemicarbazones, known as an important metal ion chelating agents, have attracted much attention from researchers because of their extensively antibacterial and antitumor activities^{21–24}, e.g., 3-aminopyridine carboxaldehyde thiosemicarbazone (3-AP) and di-2-pyridylketone-4-cyclohexyl-4-methyl-3-thiosemicarbazone (DpC). 3-AP (Fig. 1), which is in

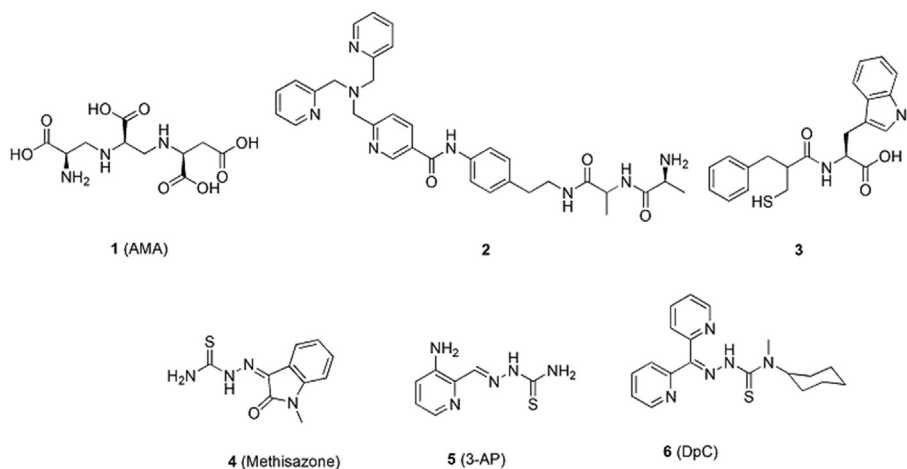


Figure 1 The structure of reported inhibitors of NDM-1 and drugs containing thiosemicarbazone.

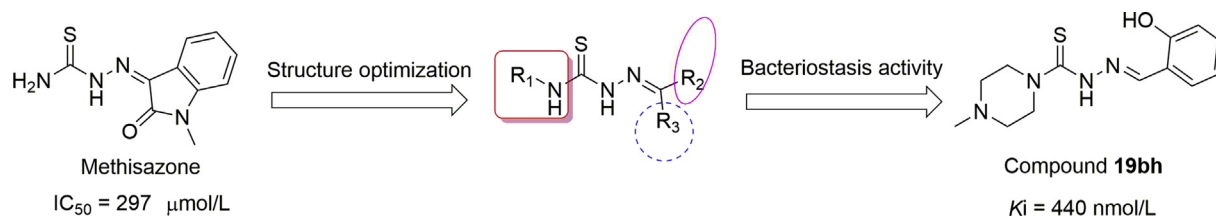
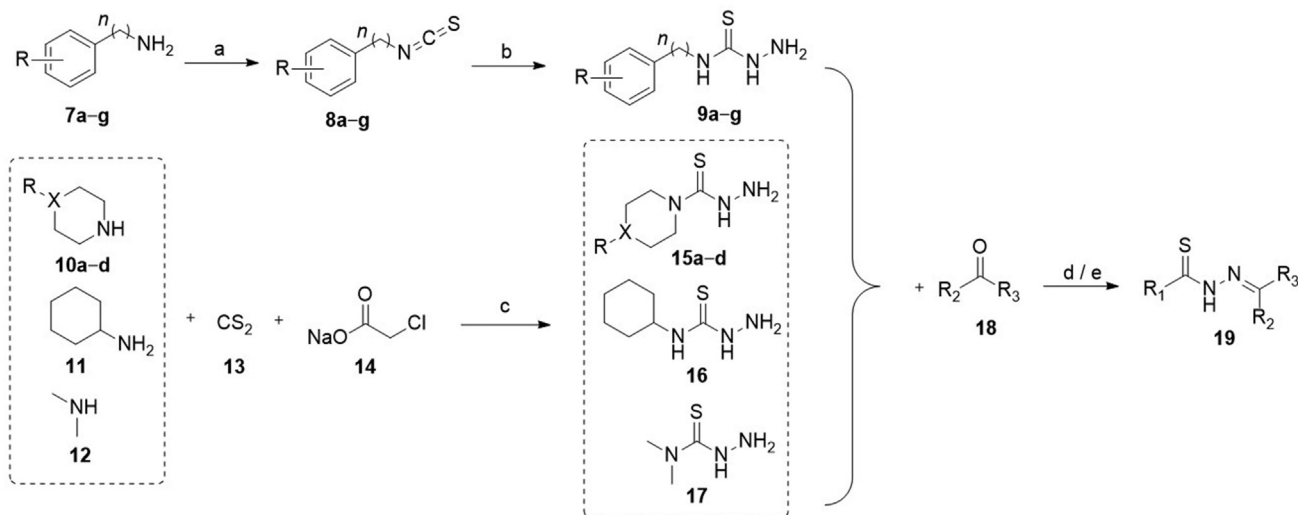


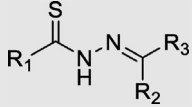
Figure 2 The strategy of structure optimization based on methisazone and bacteriostasis activity evaluation.



- n* = 0
9a R = H
9b R = *p*-OCH₃
9c R = *p*-Br
9d R = *m*-Br
9e R = *o*-Br
n = 1
9f R = H
n = 2
9g R = H
- 15a** X = O
15b X = C
15c X = N, R = *t*-Boc
15d X = N, R = CH₃
- 19a** R₁ = Phenylamino, R₂ = H, R₃ = 1-Methyl-1*H*-indol-3-yl
19b R₁ = Phenylamino, R₂ = H, R₃ = 1*H*-Indol-3-yl
19c R₁ = Phenylamino, R₂ = H, R₃ = Furan-2-yl
19d R₁ = Phenylamino, R₂ = H, R₃ = Thiophen-2-yl
19e R₁ = Phenylamino, R₂ = H, R₃ = Pyridin-2-yl
19f R₁ = Phenylamino, R₂ = H, R₃ = Pyridin-3-yl
19g R₁ = Phenylamino, R₂ = H, R₃ = Pyridin-4-yl
19h R₁ = Phenylamino, R₂ = H, R₃ = 6-Bromopyridin-2-yl
19i R₁ = Phenylamino, R₂ = H, R₃ = 5-Bromopyridin-2-yl
19j R₁ = 4-Methoxyphenylamino, R₂ = H, R₃ = Pyridin-2-yl
19k R₁ = 4-Bromophenylamino, R₂ = H, R₃ = 5-Bromopyridin-2-yl
19l R₁ = 4-Methoxyphenylamino, R₂ = H, R₃ = 1*H*-Indol-3-yl
19m R₁ = 4-Bromophenylamino, R₂ = H, R₃ = Pyridin-2-yl
19n R₁ = 4-Bromophenylamino, R₂ = H, R₃ = 5-Chloropyridin-2-yl
19o R₁ = 4-Bromophenylamino, R₂ = H, R₃ = 1*H*-Indol-3-yl
19p R₁ = 4-Bromophenylamino, R₂ = H, R₃ = 1-Methyl-1*H*-indol-3-yl
19q R₁ = 3-Bromophenylamino, R₂ = H, R₃ = Pyridin-2-yl
19r R₁ = 2-Bromophenylamino, R₂ = CH₃, R₃ = Pyridin-2-yl
19s R₁ = 4-Methoxyphenylamino, R₂ = CH₃, R₃ = Pyridin-2-yl
19t R₁ = 4-Bromophenylamino, R₂ = CH₃, R₃ = Pyridin-2-yl
19u R₁ = 2-Bromophenylamino, R₂ = CH₂CH₃, R₃ = Pyridin-2-yl
19v R₁ = 2-Bromophenylamino, R₂ = CH₂CH₂CH₃, R₃ = Pyridin-2-yl
19w R₁ = 2-Bromophenylamino, R₂ = CH(CH₃)₂, R₃ = Pyridin-2-yl
19x R₁ = 2-Bromophenylamino, R₂ = Phenyl, R₃ = Pyridin-2-yl
19y R₁ = 4-Bromophenylamino, R₂ = Pyridin-2-yl, R₃ = Pyridin-2-yl
19z R₁ = Benzylamino, R₂ = H, R₃ = Pyridin-2-yl
19aa R₁ = Phenethylamino, R₂ = H, R₃ = Pyridin-2-yl
19ab R₁ = Phenylamino, R₂ = H, R₃ = 2-Hydroxyphenyl
19ac R₁ = Phenylamino, R₂ = CH₃, R₃ = Pyridin-2-yl
19ad R₁ = Phenylamino, R₂ = CH₃, R₃ = 5-Chloro-2-hydroxyphenyl
19ae R₁ = Phenyl, R₂ = H, R₃ = 2-Hydroxyphenyl
19af R₁ = Phenyl, R₂ = CH₃, R₃ = 5-Chloro-2-hydroxyphenyl
19ag R₁ = Morpholinyl, R₂ = H, R₃ = Pyridin-2-yl
19ah R₁ = Morpholinoethylamino, R₂ = H, R₃ = Pyridin-2-yl
19ai R₁ = Piperidinyl, R₂ = H, R₃ = Pyridin-2-yl
19aj R₁ = Cyclohexylamino, R₂ = CH₃, R₃ = Pyridin-2-yl
19ak R₁ = Dimethylamino, R₂ = CH₃, R₃ = Pyridin-2-yl
19al R₁ = Morpholinyl, R₂ = CH₃, R₃ = 2-Aminophenyl
19am R₁ = Morpholinyl, R₂ = H, R₃ = Phenyl
19an R₁ = Morpholinyl, R₂ = H, R₃ = 2-Hydroxyphenyl
19ao R₁ = Morpholinyl, R₂ = H, R₃ = Pyridin-2-yl
19ap R₁ = Morpholinyl, R₂ = H, R₃ = 4-Bromophenyl
19aq R₁ = Morpholinyl, R₂ = H, R₃ = Naphthalen-2-yl
19ar R₁ = Morpholinyl, R₂ = H, R₃ = 1*H*-Indol-3-yl
19as R₁ = Morpholinyl, R₂ = H, R₃ = 5-Bromopyridin-2-yl
19at R₁ = Morpholinyl, R₂ = H, R₃ = 3,5-Dibromo-2-hydroxyphenyl
19au R₁ = Morpholinyl, R₂ = H, R₃ = 5-Chloro-2-hydroxyphenyl
19av R₁ = Morpholinyl, R₂ = H, R₃ = 5-Chloro-2-hydroxyphenyl
19aw R₁ = Morpholinyl, R₂ = H, R₃ = 3,4,5-Trimethoxyphenyl
19ax R₁ = Morpholinyl, R₂ = H, R₃ = 1-Hydroxynaphthalen-2-yl
19ay R₁ = Morpholinyl, R₂ = H, R₃ = 3-Hydroxyphenyl
19az R₁ = Morpholinyl, R₂ = H, R₃ = 4-Hydroxyphenyl
19ba R₁ = Piperazinyl, R₂ = H, R₃ = 2-Hydroxyphenyl
19bb R₁ = Piperazinyl, R₂ = H, R₃ = 2-Methoxyphenyl
19bc R₁ = Piperazinyl, R₂ = H, R₃ = 2-Ethoxyphenyl
19bd R₁ = *N*-Methylpiperazinyl, R₂ = H, R₃ = 2-Hydroxyphenyl
19be R₁ = *N*-Methylpiperazinyl, R₂ = H, R₃ = 2-Methoxyphenyl
19bf R₁ = *N*-Methylpiperazinyl, R₂ = H, R₃ = 2-Ethoxyphenyl

Scheme 1 Synthesis of the thiosemicarbazone derivatives. Reagents and conditions: (a) CS₂, Et₃N, (Boc)₂O, DMAP, THF, r.t.; (b) hydrazine hydrate (80%, w/w), methanol, reflux; (c) sodium hydroxide, hydrazine hydrate (80%, w/w), water, reflux; (d) AcOH, methanol, reflux; (e) conc. HCl, dioxane, r.t.

Table 1 Structures of compounds and size of the bacteriostatic zone (SAR part 1).



Compd.	R ₁	R ₂	R ₃	Δ _{MEM+EDTA} (mm)	Δ _{MEM+Compd.} (mm)
19a		H		8.91	1.36
19b		H		8.92	0.16
19c		H		8.58	0.12
19d		H		8.58	0.12
19e		H		9.24	2.14
19f		H		9.24	0.04
19g		H		10.7	0.66
19h		H		9.88	-0.02
19i		H		9.88	0.64
19j		H		8.24	0.78
19k		H		11.02	0.74
19l		H		10.70	0.92
19m		H		12.32	3.82
19n		H		11.78	0.68
19o		H		11.54	1.36
19p		H		8.32	-0.30
19q		-CH ₃		8.38	1.14
19r		-CH ₃		8.38	3.93
19s		-CH ₃		11.54	2.74
19t		-CH ₃		8.24	0.22
19u		-C ₂ H ₅		10.52	2.2
19v		-C ₃ H ₇		11.16	0.79
19w		-CH(CH ₃) ₂		11.23	0.13

Table 1 (continued)

Compd.	R ₁	R ₂	R ₃	Δ _{MEM+EDTA} (mm)	Δ _{MEM+Compd.} (mm)
19x		H		10.96	0.26
19y				9.60	0.31

Δ_{MEM+EDTA} means the difference of bacteriostatic zone between MEM combined using with EDTA and MEM alone; Δ_{MEM+Compd.} says the difference of bacteriostatic zone between MEM combined using with compound and MEM alone.

clinical phase II studies, is a potent ribonucleotide reductase inhibitor for the treatment of non-small-cell lung cancer and renal carcinoma^{25–29}. DpC has been in clinical phase I trials and performs good therapeutic effect for head and neck squamous cell carcinoma^{30,31}.

Recently, studies have found that these analogs have specific antibacterial activity, such as compound **4** (methisazone), an old drug (Fig. 1), containing thiosemicarbazone and isatin structural skeleton, which had weak inhibitory activity against NDM-1¹³. However, the structure–activity relationship (SAR) studies as well

as the mechanism of action were rarely explored, especially in antibiotics. Previously, we have reported that some compounds with thiosemicarbazone skeletons performed a good antitumor activity^{32,33}. In the present study, SAR based on thiosemicarbazones against NDM-1-producing Enterobacteriaceae was studied systematically (Fig. 2). Noteworthy, the thiosemicarbazone derivatives **19bg** and **19bh** were potent NDM-1 inhibitors that could restore the susceptibility of the meropenem (MEM) against clinical isolates. And the combination of compound **19bh** and MEM was markedly effective in treating infections caused by NDM-1 positive strain and

Table 2 Structures of compounds and size of the bacteriostatic zone (SAR part 2).

Compd.	R ₁	R ₂	R ₃	Δ _{MEM+EDTA} (mm)	Δ _{MEM+Compd.} (mm)
19z		H		9.28	0.02
19aa		H		9.52	0.06
19ab		H		9.62	0.24
19ac		–CH ₃		10.75	1.56
19ad		–CH ₃		8.22	0.88
19ae		H		9.23	1.38
19af		–CH ₃		9.22	0.06
19ag		–CH ₃		10.68	6.32
19ah		H		10.60	1.34
19ai		H		13.12	5.75
19aj		–CH ₃		12.05	0.62
19ak		–CH ₃		12.52	3.62

Δ_{MEM+EDTA} means the difference of bacteriostatic zone between MEM combined using with EDTA and MEM alone; Δ_{MEM+Compd.} says the difference of bacteriostatic zone between MEM combined using with compound and MEM alone.

Table 3 Structures of compounds and size of the bacteriostatic zone (SAR part 3).

Compd.	R ₁	R ₂	R ₃	Δ _{MEM+EDTA} (mm)	Δ _{MEM+ Compd.} (mm)
19al		-CH ₃		11.22	1.96
19am		-CH ₃		8.58	3.02
19an		H		11.22	11.34
19ao		H		8.96	5.62
19ap		H		9.56	0.62
19aq		H		9.56	1.58
19ar		H		11.87	8.42
19as		H		13.12	6.43
19at		H		10.32	0.72
19au		H		10.32	1.10
19av		-CH ₃		8.58	0.10
19aw		H		9.76	4.34
19ax		H		12.02	0.74
19ay		-CH ₃		8.72	0.64
19az		-CH ₃		8.72	3.26

Δ_{MEM+EDTA} means the difference of bacteriostatic zone between MEM combined using with EDTA and MEM alone; Δ_{MEM+Compd.} says the difference of bacteriostatic zone between MEM combined using with compound and MEM alone.

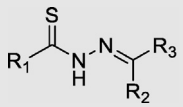
prolonging the survival time of sepsis mice. Herein, we reported the results of our studies that ultimately led to the discovery of thiosemicarbazone derivatives as possible leads.

2. Results and discussion

2.1. Chemistry

The general route for the synthesis of the target thiosemicarbazone derivatives referred to the Schiff base mechanism (Scheme 1). As shown, the hydrazine carbothioamide intermediates were prepared by two routes, with phenylamine and aliphatic amine as the starting reagents respectively. Firstly, commercially available substituted anilines **7a–g**, Et₃N and **13** were mixed in tetrahydrofuran (THF) at

room temperature (r.t.), following by adding di-*tert*-butyl dicarbonate ((Boc)₂O) and 4-dimethylaminopyridine (DMAP) for a one-pot reaction to provide **8a–g** with 45%–70% yield. Then, the mixture of hydrazine hydrate and **8a–g** was refluxed in methanol, compounds **9a–g** were afforded in 65%–85% yield. On the other hand, compounds **10a–d** were mixed with sodium hydroxide in water, then added **13** and **14** in order, the hydrazine hydrate was added finally and the mixture refluxed and crystallized to get corresponding intermediates **15a–d** with 40%–55% yield. Likewise, compounds **16** and **17** were derived from reagents **11** and **12** respectively. Finally, appropriate aldehyde or ketone **18** was mixed with the prepared *N*-substituted hydrazine carbothioamide intermediates in methanol and refluxed after addition of a catalytic amount of acetic acid (AcOH), the precipitation was filtered, and

Table 4 Structures of compounds and size of the bacteriostatic zone (SAR part 4).


Compd.	R ₁	R ₂	R ₃	Δ _{MEM+EDTA} (mm)	Δ _{MEM+Compd.} (mm)
19ba		H		10.62	15.16
19bb		H		10.42	13.76
19bc		H		12.14	14.12
19bd		H		8.22	15.50
19be		H		8.54	12.62
19bf		H		8.54	10.42
19bg		Hydrochloride of compd. 19ba		11.14	15.20 ^a
19bh		Hydrochloride of compd. 19bd		10.44	12.74 ^a

^aThe average value of three separate experiments; Δ_{MEM+EDTA} means the difference of bacteriostatic zone between MEM combined using with EDTA and MEM alone; Δ_{MEM+Compd.} says the difference of bacteriostatic zone between MEM combined using with compound and MEM alone.

purified by recrystallization or column chromatography to provide target compound **19** with yield ranging from 50% to 85%. Noteworthy, individual products needed to undergo de-protection process to remove the *tert*-butoxy carbonyl (Boc) group with concentrated hydrochloric acid (conc. HCl).

The chemical structure characterization of all target compounds was confirmed by ¹H NMR, ¹³C NMR and high-resolution mass spectra (HR-MS). Besides, these target thiosemicarbazone derivatives could possess either *E* or *Z* isomeric form because of the existence of azomethine (–CR=N–) moiety, which can be explained by 2D NOESY NMR. In ¹H NMR spectra, the typical singlet signals were observed with chemical shifts ranging from δ 9.48 to 14.33 ppm (1H, hydrazine-NH) and δ 8.08 to 9.40 ppm (1H, –CH=N–); in the ¹³C NMR spectra, the chemical shift of C=N moiety appeared to range from δ 138.45 to 178.02 ppm and C=S moiety appeared at the region of δ 162.79–188.17 ppm. These data were all consistent with the previous reports involving thiosemicarbazone^{34,35}. Additionally, in the ¹H NMR spectrum analysis, the –CH=N– signal was observed as a single peak for the singlet azomethine hydrogen, indicating that only one isomer was generated. To confirm the stereochemistry more accurately, compound **19ba** was chosen to elucidate this isomerism by 2D NOESY NMR. In the NOESY spectra of compound **19ba**, the spatial correlation between azomethine (–CH=N–) at δ 8.41 ppm and the hydrogen of hydrazine at δ 12.06 ppm was observed, indicating that only *E* isomer existed because of the appropriate intramolecular H–H distance (Supporting Information Figs. S1 and S2). Collectively, these results could prove the successful

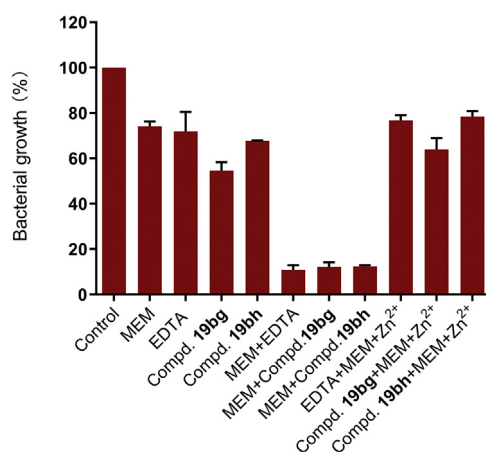
NDM-1-containing *Klebsiella pneumoniae*

Figure 3 Metal suppression experiments. Bacterial growth rates of NDM-1-positive *K. pneumoniae* with monotherapy treatment groups (MEM = 2 μg/mL, EDTA = 32 μg/mL, compound **19bg** = 32 μg/mL and compound **19bh** = 32 μg/mL). The concentration of each component in the combination groups was the same as that in the monotherapy treatment groups, except Zn²⁺ was provided by ZnCl₂ (32 μg/mL); bacterial growth rate was denoted as the mean ± SD (*n* = 3).

synthesis of the target compounds and indicate that the target compounds were unambiguously confirmed as *E* isomer.

2.2. Antibacterial activity and SAR studies

Agar disk diffusion assay was conducted initially to evaluate the inhibitory activity of all synthesized compounds combined with MEM against the NDM-1 positive *Escherichia coli* strain, and ethylene diamine tetraacetic acid (EDTA) was used as the positive control^{36,37}. The difference of bacteriostatic zone between MEM combined using with EDTA or candidate compounds and MEM alone was shown in Tables 1–4.

Firstly, we attempted to replace the isatin part to examine the contribution of thiosemicarbazone pharmacophore to the bacteriostatic activity, the SAR studies of thiosemicarbazone derivatives were performed on the R₂ and R₃ position, leading to the formation of compounds **19a–y** (Table 1). Compounds **19a–i** were designed to investigate the SAR of R₃ position, where different aromatic heterocyclic rings were screened, such as pyridine, furan, thiophene and indole ring. Clearly, most compounds had no noticeable antimicrobial effect (Δ_{zoom} < 4.0 mm). Only compound **19e** containing 2-pyridyl exhibited very weak bacteriostatic activity, the difference of bacteriostatic zone between compound **19e** combined MEM and MEM alone was 2.14 mm. Besides, it was observed that when the substituted site of pyridyl changed from 2- to 3- or 4-position, the antimicrobial effect decreased significantly (**19e** vs. **19f** and **19g**). In-depth structural optimization focusing on replacement of R₂ groups affiliated the thiosemicarbazone core was performed. As shown in Table 1, the effect of methyl substitution at R₂ position on the activity seemed to be uncertain (**19m** > **19t**, but **19j** < **19s**). To further study this, different alkyl modifications were led in, and the

Table 5 MIC ($\mu\text{g/mL}$) of MEM-inhibitors combination against NDM-1 positive clinical isolates.

No. of CRE	Bacteria species ^a	MIC ($\mu\text{g/mL}$)													
		EDTA		19bg		19bh		MEM		MEM/EDTA ^b		MEM+19bg		MEM+19bh	
		64	64	64	64	64	32	64	32	64	32	64	32	64	
1	<i>Klebsiella pneumoniae</i>	>64	>64	>64	64	2	0.06	1	<0.03	0.5	<0.03	<0.03	<0.03		
2	<i>Klebsiella pneumoniae</i>	>64	>64	>64	32	0.06	<0.03	<0.03	<0.03	<0.03	<0.03	<0.03	<0.03		
3	<i>Klebsiella pneumoniae</i>	>64	>64	>64	32	1	<0.03	0.125	<0.03	0.06	<0.03	<0.03	<0.03		
4	<i>Enterobacter cloacae</i>	>64	>64	>64	32	1	0.25	0.5	0.06	0.125	<0.03	<0.03	<0.03		
5	<i>Enterobacter cloacae</i>	>64	>64	>64	8	0.125	0.06	0.25	<0.03	0.06	<0.03	<0.03	<0.03		
6	<i>Escherichia coli</i>	>64	>64	>64	32	0.25	<0.03	1	<0.03	0.5	<0.03	<0.03	<0.03		
7	<i>Klebsiella oxytoca</i>	>64	>64	>64	32	0.125	0.06	0.25	<0.03	0.125	<0.03	<0.03	<0.03		
8	<i>Klebsiella oxytoca</i>	>64	>64	>64	16	1	0.06	0.5	<0.03	0.25	<0.03	<0.03	<0.03		
9	<i>Citrobacter freundii</i>	>64	>64	>64	64	0.06	<0.03	<0.03	<0.03	0.125	<0.03	<0.03	<0.03		
10	<i>Providencia ewing</i>	>64	>64	>64	32	0.5	<0.03	<0.03	<0.03	<0.03	<0.03	<0.03	<0.03		

^aAll of the strains tested were isolated from clinical Enterobacteriaceae bacteria producing NDM-1 enzyme.

^bThe concentration of EDTA in the combined susceptibility test was fixed also at 32 and 64 $\mu\text{g/mL}$.

results showed that the activity decreased with the length of alkyl chain increasing (**19r** vs. **19u** and **19v**). Also, the phenyl substitution resulted in a significant loss of potency (**19x**, $\Delta\text{zoom} = 0.26$ mm). Meanwhile, when R_2 was pyridyl, the activity was about 10-fold weaker than corresponding no-substituted (**19m** vs. **19y**). Thus, these results implied that appropriate sterically hindered effect of substitution at R_2 location was critical for the antibacterial activity. And so far, changing substituents on R_2 position appeared to be in vain, so we did not attempt other groups except methyl any more.

Based on the first-round of optimization results, the second-round structural modification primarily focused on the variations of R_1 . As shown in Table 1, we have tried to introduce different amendment at R_1 -phenyl to develop the activity, but unfortunately, it was little success. Inspired by wondering whether the change to the original scaffold of R_1 would improve the activity, we initially tried to explore the effect of the carbon chain length between R_1 -phenyl and thiocarbamide N-terminal to the activity. As shown in Table 2, when the spacer extended to either one- or two-carbon, the activity all reduced obviously (**19e** vs. **19z** and **19aa**).

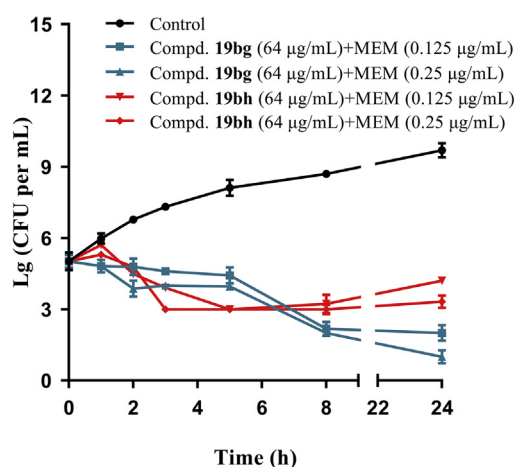


Figure 4 The time-dependent killing of bacterial by MEM combined with compound **19bg** or **19bh**. NDM-1 enzyme-producing *K. pneumoniae* was challenged with compounds **19bg** and **19bh** combined with MEM.

Subsequently, we attempted to replace the phenyl by an aliphatic ring or an alkyl group. Among which, compound **19ag** bearing morpholinyl exhibited good antimicrobial effect with an about 1.61-fold increase in the size of the bacteriostatic zone, comparable to compound **19r** ($\Delta\text{zoom} = 3.93$ mm). Similarly, compound **19ai** with piperidinyl substituted also displayed favorable activity ($\Delta\text{zoom} = 5.75$ mm), but was slightly weaker than compound **19ag**. In this view, following structure optimization was based on R_1 being morpholine group.

As shown in Table 3, several compounds have shown excellent activity, suggesting that morpholinyl was indeed much tolerated than original phenyl. This might be due to the enhancement of the water solubility. It was noticed that 2-pyridyl at R_3 position was still beneficial for the activity, such as **19ao** and **19as**, which showed high potency. Interestingly, replacement of the 2-pyridyl with 2-hydroxyphenyl resulted in a robust increase of antimicrobial activity (**19an** vs. **19ao**) comparing with the control EDTA. Moreover, when the substituted site of phenyl changed from 2- to 3- or 4-position, namely **19ay** and **19az**, the activity decreased.

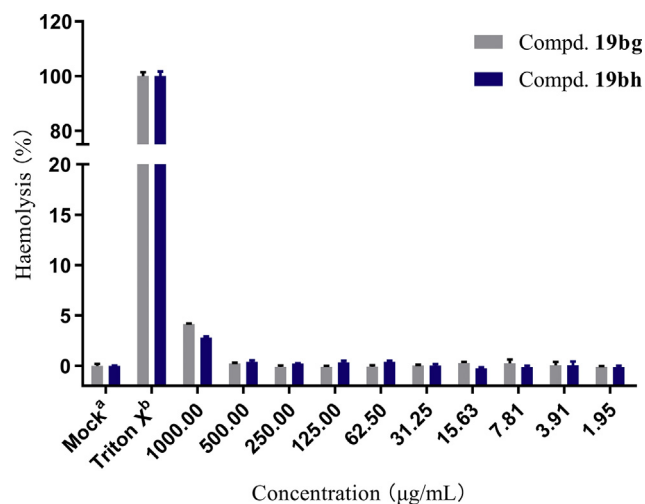


Figure 5 Hemolysis rate of red blood cells treated with different concentrations of compounds **19bg** and **19bh**. Mock^a: treated with phosphate-buffered saline (PBS); Triton X^b: treated with 0.5% Triton X-100 detergent. Hemolysis rate is the mean \pm SD ($n = 3$).

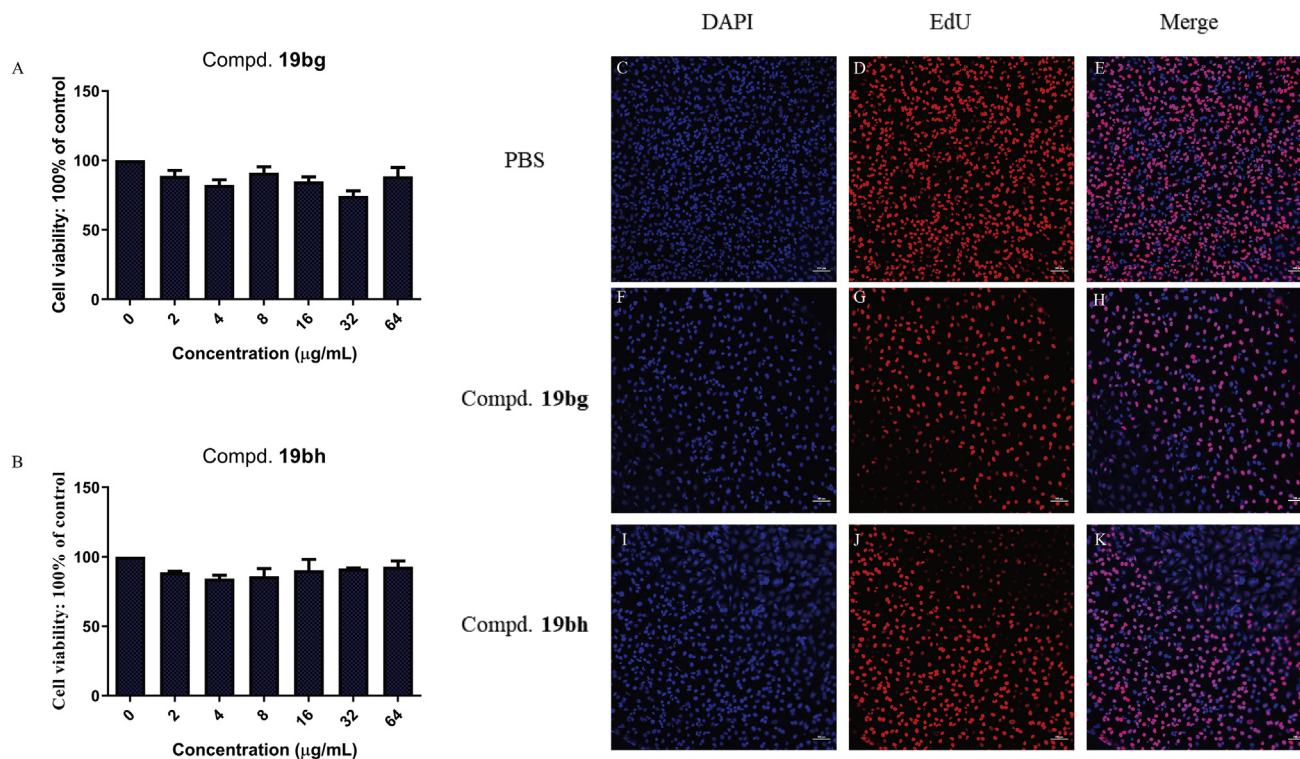


Figure 6 Cell viability and fluorescence microscopy images of HeLa cells after treatment with compound **19bg** or **19bh** for 48 h and staining with EdU and DAPI. (A) and (B) Cell viability of HeLa cells treated with compounds **19bg** and **19bh**, respectively; (C)–(E) non-treated HeLa cells (control group); (F)–(H) cells treated with compound **19bg** (64 µg/mL); (I)–(K) cells treated with compound **19bh** (64 µg/mL). The observation of the fixed and stained cells was performed with an Olympus laser scanning confocal microscope, magnification $\times 200$. The photomicrographs shown are representative of at least two independent experiments performed.

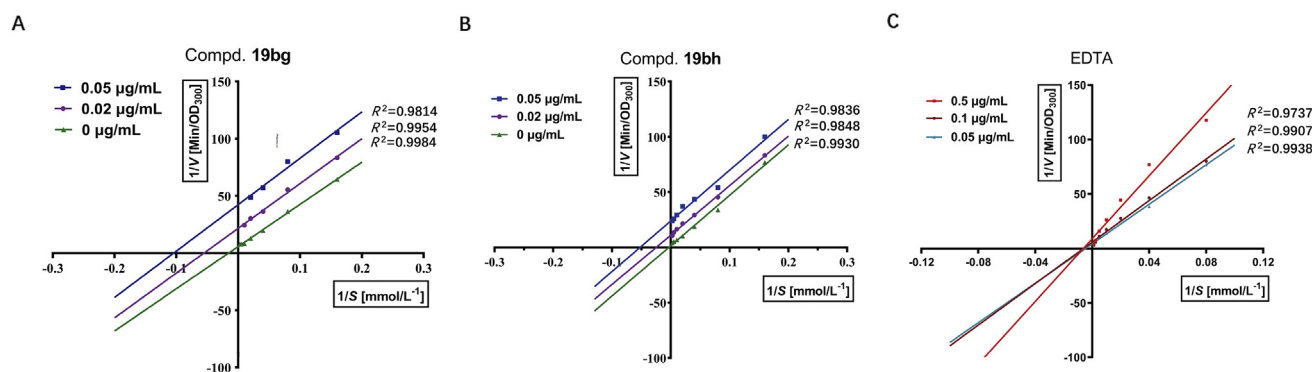


Figure 7 Lineweaver–Burk plots of inhibition of the NDM-1 hydrolysis activity by compounds **19bg** and **19bh**. The concentrations (µg/mL) of inhibitors (A) compound **19bg**, 0 (▲), 0.02 (●), and 0.05 (■); (B) Compound **19bh**, 0 (▲), 0.02 (●), and 0.05 (■); (C) EDTA, 0.05 (▲), 0.1 (●), and 0.5 (■).

This phenomenon was similar to 2-pyridine substitution which was discussed above. While, the amino group, bearing similar polarity to the hydroxyl group, did not contribute to the activity (**19al**, $\Delta_{\text{zoom}} = 1.96$ mm). Besides, when the hydroxyl group was at the same substituted site, quinoline group, namely compound **19ax**, displayed very weak efficacy.

As discussed above, the water solubility of these thiosemicarbazone derivatives was vital for the bacteriostatic activity. Inspired by this, further optimization focused on introducing hydrophilic groups to the scaffold, *e.g.*, piperazinyl or *N*-methyl piperazinyl. Also, we tried to use alkyl group (methyl and ethyl) to

modify the hydroxyl group of R_3 position to improve the water solubility, the results were shown in Table 4. In comparison to morpholinyl, piperazinyl was likely a better choice, owing to the robust improvement of the activity. All the compounds showed more substantial effect than EDTA. In addition, we did observe that the modification of the hydroxyl group of R_3 position led to a slight loss of activity (**19ba** vs. **19bb** and **19bc**, **19bd** vs. **19be** and **19bf**).

In a word, a total of 7 compounds exhibited better activities than the positive control EDTA to increase the susceptibility of NDM-1 producing isolate to MEM. Moreover, compounds **19ba**

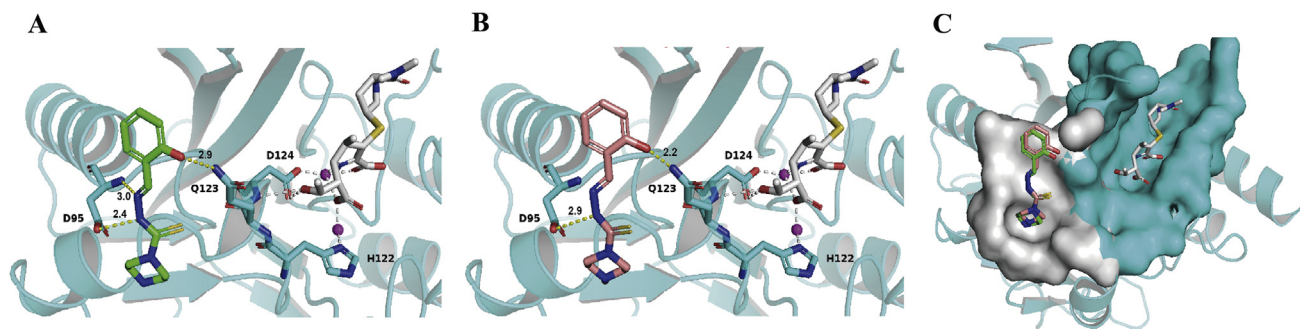


Figure 8 Overview of ligand-binding sites of compounds **19bg** and **19bh** in human NDM-1 and the detailed interactions. Small molecules were shown as sticks. Protein NDM-1 (PDB ID: 5N0H) was shown as cartoon (cyan), for clarity, NDM-1 was shown in 50% transparent cartoon. NDM-1 residues interacting with compounds were shown as sticks, hydrogen bonds were shown as dashed lines (yellow), Zn^{2+} ions shown as spheres (magenta). (A) Interaction model of compound **19bg** in NDM-1. Three hydrogen bonds between **19bg** (green) and NDM-1 residues were shown, bonds length were also marked. The interactions (grey) between hydrolyzed MEM (grey) and NDM-1 residues were displayed partly. (B) Interaction model of compound **19bh** in NDM-1. Two hydrogen bonds between **19bh** (salmon) and NDM-1 residues were shown, bonds length were also marked. (C) By comparison, compounds **19bg** and **19bh** occupied the same allosteric binding pocket (grey) in NDM-1, the hydrolyzed MEM occupied the substrate binding pocket (cyan) in NDM-1. These two binding pockets were closely adjacent.

and **19bd** showed the most potent effect. To further enhance the hydrophilicity, we made those two compounds into hydrochloride form to yield compounds **19bg** and **19bh**, which performed similar antibacterial effect (results of agar disk diffusion assay was shown in Supporting Information Fig. S3). Based on these observations, we supposed that these compounds containing thiosemicarbazone might serve as NDM-1 inhibitors by chelating zinc ion like EDTA, and compounds **19bg** and **19bh** were selected for further investigation.

2.3. Zinc homeostasis test

It has been documented that chelation of zinc ions, which played a vital role in maintaining the hydrolytic activity of NDM enzymes, by EDTA led to the inactivation of NDM-1^{36,37}. Thus, zinc homeostasis testing was employed to verify whether compounds **19bg** and **19bh** could exert an inhibitory effect on NDM-1 enzyme by chelation of Zn^{2+} . Bacterial growth rates of NDM-1 positive *Klebsiella pneumoniae* in different treating groups including monotherapy treatment groups (MEM, EDTA, compound **19bg** and compound **19bh**), MEM-inhibitors combination groups (MEM + EDTA, MEM+**19bg** and MEM+**19bh**) and untreated group (control) were shown in Fig. 3. Of note, combination use of MEM and one of the inhibitors EDTA, **19bg** or **19bh** led to a sharp decrease of the bacterial growth rates comparing with the control group, indicating compounds **19bg** and **19bh** exhibited good inhibition on NDM-1 enzyme. While, adding additional zinc ions to these combinations caused the bacterial growth rates raised again, comparable with the results of monotherapy treatment groups, suggesting that the presence of extra zinc ions could influence the activity of these inhibitors and maintain the hydrolytic activity of NDM-1 against MEM.

2.4. Minimum inhibitory concentration (MIC) of MEM-inhibitors combination against clinical NDM-producing isolates

Antimicrobial susceptibility testing was conducted by using microbroth dilution method according to Clinical and Laboratory Standards Institute (CLSI) guidelines M07-A9 to determine the MIC of compounds **19bg** and **19bh** in combination with MEM

against NDM-1 producing Enterobacteriaceae isolates. All of the 10 non-duplicated MEM resistant isolates ($\text{MIC} \geq 16 \mu\text{g/mL}$) which were recovered from a teaching hospital of Zhengzhou University (Zhengzhou, China) were confirmed carrying NDM-1-gene by PCR and sequencing methods.

As shown in Table 5, when the inhibitors were added at the concentration of $32 \mu\text{g/mL}$, both of MEM + compound **19bg** ($\text{MIC}_{90} = 1 \mu\text{g/mL}$) and MEM + compound **19bh** ($\text{MIC}_{90} = 0.5 \mu\text{g/mL}$) combinations showed comparable activities as MEM + EDTA ($\text{MIC}_{90} = 1 \mu\text{g/mL}$) to restore activity of MEM against NDM-1 producing isolates. While, when the concentration of inhibitors increased to $64 \mu\text{g/mL}$, either combination of MEM + compound **19bg** or MEM + compound **19bh** ($\text{MIC}_{90} < 0.03 \mu\text{g/mL}$) exhibited better effect than MEM + EDTA ($\text{MIC}_{90} = 0.06 \mu\text{g/mL}$) for rescuing MEM activity.

2.5. Bactericidal kinetics

To further study the antibacterial timeliness of these two compounds, bactericidal killing kinetics assay was employed to evaluate activities of compound **19bg** or **19bh** together with MEM against NDM-1 producing strain. As shown in Fig. 4, combination use of **19bh** and MEM performed excellent bactericidal activity, led to a 3 log populations reduction of NDM-1 producing strain within 24 h.

2.6. Toxicity analysis

2.6.1. Hemolytic activity

Since compounds **19bg** and **19bh** had an excellent antibacterial effect, we evaluated those two compounds for hemolysis activity. The results of hemolytic activities were shown in Fig. 5. The red blood cells (RBCs) hemolysis rates of compounds **19bg** and **19bh** were lower than 5% even at an extremely high concentration of 1000 mg/mL , indicating both of which exhibited no toxicity to RBCs.

2.6.2. Cytotoxicity

To further investigate the cytotoxicity of these compounds, HeLa cells were treated respectively with **19bg** and **19bh** at the concentrations with a range of $0\text{--}64 \mu\text{g/mL}$ for 48 h. Then, a CCK-8 assay kit was used to detect the anti-proliferation effect of the

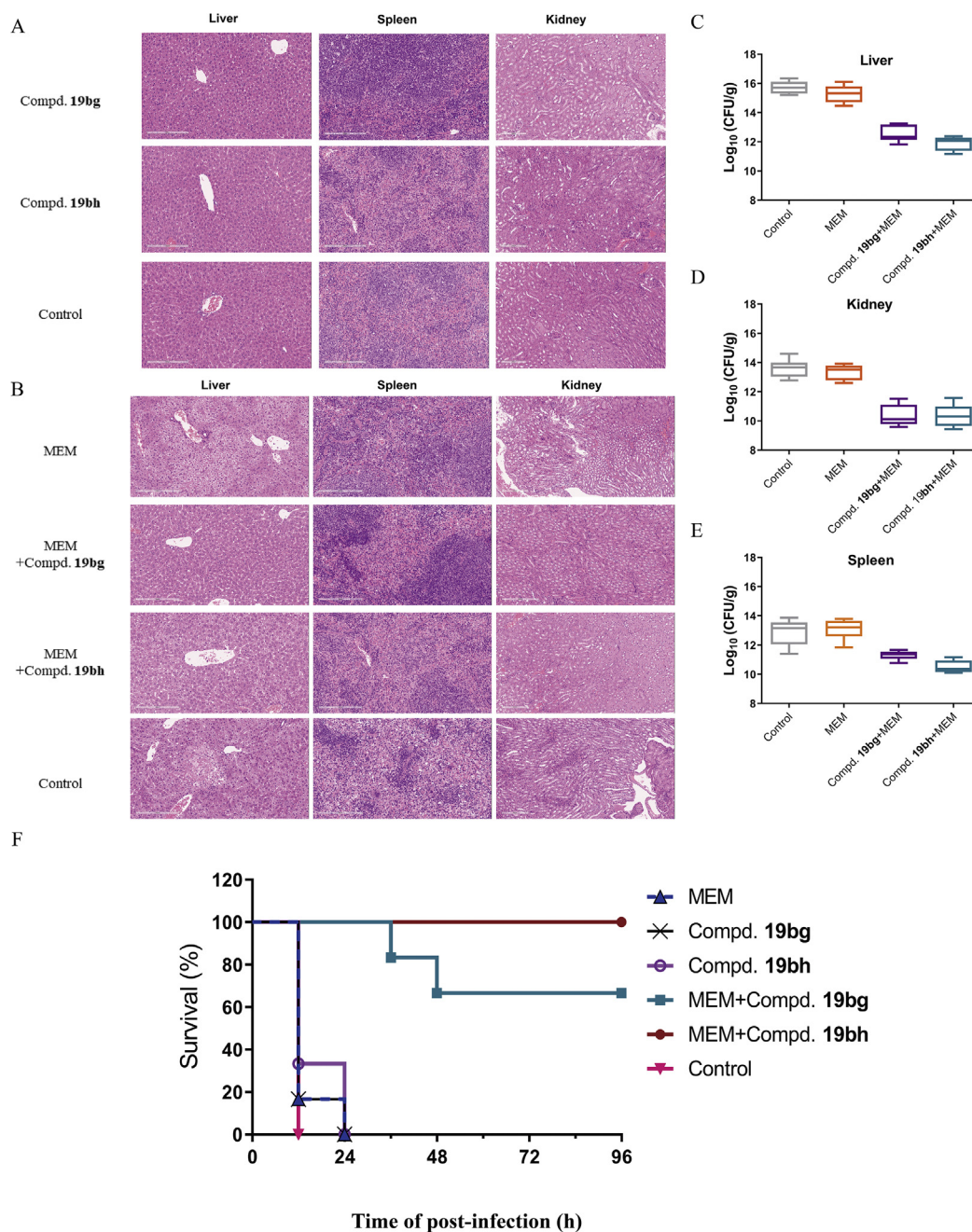


Figure 9 Safety evaluation of compounds **19bg** and **19bh** and their rescue MEM activity *in vivo*. (A) For safety evaluation experiments, BALB/c mice were given a single dose of compound **19bg** (64 mg/kg), compound **19bh** (64 mg/kg) or PBS by subcutaneous injection. Data was the means \pm standard error (SE) from three separate experiments ($n = 2$ per group). (B) H&E staining results of BALB/c mice were given a median lethal dose (5×10^6 CFU) of NDM-1 positive *K. pneumoniae* by intraperitoneal injection and treated with a single dose of MEM (10 mg/kg) and combination of MEM (10 mg/kg) plus compound **19bg** (10 mg/kg), compound **19bh** (10 mg/kg) or PBS by subcutaneous injection. (C)–(E) Bacterial load in the liver, spleen and kidney of NDM-1 positive *K. pneumoniae* infected BALB/c mice with different treatment approaches were determined by selective plating. Data was the means \pm SE from four separate experiments ($n = 6$ per group). (F) For survival experiments, BALB/c mice were given a lethal dose (1×10^7 CFU) of *K. pneumoniae* by intraperitoneal injection and treated with a single dose of MEM (10 mg/kg), compound **19bg** (30 mg/kg), compound **19bh** (30 mg/kg) and combination of MEM (10 mg/kg) plus compound **19bg** (30 mg/kg) or compound **19bh** (30 mg/kg), or PBS by subcutaneous injection. Data was the means \pm SE from six separate experiments ($n = 6$ per group).

different concentration of the two compounds, and results were shown in Fig. 6A and B. The half-maximal inhibitory concentrations (IC₅₀) of the two compounds were found to be more than 64 μ g/mL.

Furthermore, in order to confirm the results shown in Fig. 6A and B, an immunofluorescent staining assay, by using the EdU cell proliferation kit, was conducted to determine whether the DNA synthesis in living cells could be affected by these two compounds.

As shown in Fig. 6, the results clearly showed that, after treatment by compound **19bg** (Fig. 6F–H) or **19bh** (Fig. 6I–K) with the concentration of 64 $\mu\text{g/mL}$, there were more than 50% cells survived when compared with untreated control (Fig. 6C–E). These results indicated that the NDM-1 inhibitors exerted low toxicity against HeLa cells. hERG inhibition of candidate compounds (result was shown in Supporting Information Table S1) indicated compounds **19bg** and **19bh** performed very low hERG inhibitory activity and they are not considered to increase the risk of drug-induced long QT syndrome (LQTS).

2.7. Inhibition on NDM-1

We have identified compounds **19bg** and **19bh** as the most potent antibacterial agents in combination with MEM against clinical $bla_{\text{NDM-1}}$ -producing isolates among our synthesized compounds. The NDM-1 protein was expressed and purified for evaluating the inhibit activities of compounds **19bg**, **19bh** and the positive control EDTA against NDM-1 enzyme. The results showed each one had NDM-1 enzyme inhibitory action, and IC_{50} of compound **19bg**, **19bh** and EDTA were 0.233, 0.237 and 0.0837 $\mu\text{g/mL}$, respectively.

To further study the mechanism of action of these compounds, the inhibition constants K_i against NDM-1 were also determined. K_i of compounds **19bg** and **19bh** against NDM-1 were calculated to be 0.63 and 0.44 $\mu\text{mol/L}$, smaller than that of EDTA with K_i of 1.25 $\mu\text{mol/L}$. These results indicated that compounds **19bg** and **19bh** inhibited NDM-1 enzyme more effectively than EDTA.

Lineweaver–Burk Plots^{38,39} (Fig. 7) results revealed that compounds **19bg** and **19bh** acted as uncompetitive inhibitors, characterized by the formation of substrate–enzyme–inhibitor complexes with MEM and NDM-1 enzymes in bacteria, preventing NDM-1 from hydrolyzing MEM. While the EDTA was non-competitive inhibitor, with no competitive effect on the substrate, reduced the activity of the NDM-1 and binded equally well to the NDM-1 whether or not it had already bound the substrate.

2.8. Molecular docking studies

To predict the binding mode of uncompetitive inhibitors with NDM-1, our docking study was based on the X-ray structure of NDM-1 with a hydrolyzed MEM ligand (PDB ID: 5N0H). Considering that compounds **19bg** and **19bh** were uncompetitive inhibitors, we suspected that they might bind at allosteric sites of NDM-1. First, we used Cavity and CorrSite program^{40–42} to identify potential allosteric ligand binding sites, the results outputted 4 allosteric binding sites (data not show). Because H122 and D124 were critical residues for NDM-1 catalyzed carbapenem hydrolysis, D124 was directly involved in proton transport in the catalytic process⁴³. We speculated that compounds **19bg** and **19bh** were most likely to bind in the allosteric pocket (grey pocket in Fig. 8C) which was adjacent to the substrate pocket (cyan pocket in Fig. 8C).

Thus, compounds **19bg** and **19bh** were docked into the allosteric pocket (grey pocket in Fig. 8C) of NDM-1 respectively. As shown in Fig. 8A, **19bg** (colored in green) formed two H-bond interactions with D95, additional H-bond interaction was formed with Q123. Differently, as shown in Fig. 8B, compound **19bh** (colored in salmon) formed only one H-bond interaction with D95, another H-bond interaction was also formed with Q123. These H-bond lengths were labeled in Fig. 8A and B. As shown in Fig. 8C, compounds **19bg** and **19bh** were occupied the same region of the allosteric pocket, and they all formed H-bond

interaction with Q123. Q123 was between H122 and D124, which were participated in the catalytic process of substrates. We speculated that the binding of compounds **19bg** and **19bh** would affect the catalytic effect of NDM-1 on the substrate MEM.

2.9. In vivo activities of compounds 19bg and 19bh

As stated above, compounds **19bg** and **19bh** were effective uncompetitive inhibitors of NDM-1 and had good bacteriostatic effect when used in combination with MEM. Hence, we evaluated the safety and bacteriostatic activity of the compounds **19bg** and **19bh** *in vivo*. Firstly, subcutaneous injection of BALB/c mice with compound **19bg** or **19bh** at the concentration of 64 mg/kg to evaluate the safety. As shown in Fig. 9A, 24 h after injection, there was no obvious pathological change in the liver, spleen and kidney of the medicated groups by H&E staining compared with the control group. Considering the flip side, compared with the combination group, H&E staining of sepsis mice results showed that parenchymatous organs appeared degeneration and infiltration with the inflammatory cells, just like liver and kidney of control group and MEM single group. Meanwhile, the number of megakaryocyte neutrophils increased significantly in the paracortex of spleen in control group and MEM single group compared to other combination groups. As shown in Fig. 9C–E, combination therapy with candidate compounds (**19bg** and **19bh**, respectively) and MEM significantly reduced the bacterial loaded in the liver by subcutaneous injection as well as spleen and kidney.

Remarkably, the combined medicine group extended the life span of the sepsis mice and was significantly superior to the control group and MEM single group (Supporting Information Table S2). Especially, in the combination group of compounds **19bh** and MEM, no mice were killed after infecting with NDM-1 positive strain within 96 h (Fig. 9F). According to experimental data, compound **19bh** could restore the susceptibility of the MEM against NDM-1-positive *K. pneumoniae* *in vivo* and could significantly prolong the survival time of sepsis mice. The results of pharmacokinetic (PK) profiles indicated that compound **19bh** had a favorable PK property (Supporting Information Fig. S4 and Table S3).

3. Conclusions

In this study, a total of 60 thiosemicarbazone derivatives were designed and synthesized and their potential antibacterial activities against NDM-1 positive clinical isolates combined with meropenem were evaluated for SAR studies. Among them, compounds **19bg** and **19bh** exhibited promising inhibitory activity during *in vitro* antimicrobial susceptibility tests and performed good inhibitory activity against NDM-1 (IC_{50} = 0.233 and 0.237 $\mu\text{g/mL}$, respectively) with uncompetitive inhibition toward MEM–enzyme complex. Moreover, docking analysis illustrated that compounds **19bg** and **19bh** were most likely to bind in the allosteric pocket which was adjacent to the substrate pocket. In addition, the combination of compounds **19bh** and MEM was markedly effective in treating infections caused by NDM-1 positive strain and prolonging the survival time of sepsis mice with low toxicity. In summary, for the first time, a series of thiosemicarbazone-based, specific NDM-1 inhibitors were explored and exhibited significant antibacterial activities *in vivo*, which might serve as leading compounds targeting NDM-1 producing drug-resistance clinical isolates.

4. Experimental

4.1. General information

All the reagents and solvents used in the chemical synthesis were obtained from commercial sources and were used without further purification. All the chemistry reactions were monitored by thin layer chromatography (TLC) on silica gel which was purchased from Qingdao Haiyang Chemical Co., Ltd., Qingdao, China. Column chromatography was carried out at medium pressure using silica gel (200–300 mesh) purchased from Qingdao Haiyang Chemical Co., Ltd. ^1H NMR and ^{13}C NMR spectra data were obtained on Bruker AVANCE III 400 MHz spectrometer (Bruker Instruments, Inc., Ettlingen, Germany), chemical shifts (δ) were reported in parts per million (ppm) relative to tetramethylsilane (TMS) and J values were reported in Hertz (Hz). The NMR spectra data of compounds were provided in Supporting Information. High-resolution mass spectra (HR-MS) was recorded on a Waters Micromass Q-T of Micromass spectrometer by electrospray ionization (ESI; Waters Micro Q-TOF, Milford, MA, USA). The purity of the target compounds was determined by reverse-phase ultra-performance liquid chromatography (UPLC; Waters, ACQUITY H-Class, Milford, MA, USA) analysis. The signal was monitored at 235 nm with a UV detector. Water/acetonitrile served as a binary gradient mobile phase, with a flow rate of 0.3 mL/min.

4.2. Chemistry

4.2.1. General procedure for preparation of 8a–g

Available substituted anilines **7a–g** (3 mmol) were dissolved in THF (8 mL) in a 25 mL round-bottom flask, then CS_2 (30 mmol) and Et_3N (3 mmol) were added dropwise in turn. While reacting for 3 h at r.t. and monitoring *via* TLC until the complete conversion of reagents **7a–g**. The system was cooled in an ice bath, then $(\text{Boc})_2\text{O}$ (3 mmol, dissolved in 2 mL THF) and DMAP (0.03 mmol, dissolved in 0.5 mL THF) were added immediately, followed by stirring for another 0.3 h. Then the system was concentrated under reduced pressure and purified by column chromatography to provide phenyl isothiocyanates **8a–g** with 45%–70% yield.

4.2.2. General procedure for preparation of 9a–g

In a 25 mL round-bottom flask, **8a–g** (1.5 mmol) was dissolved in methanol (5 mL), following by adding hydrazine hydrate (80%, *w/w*, 4.5 mmol) dropwise, while heating under reflux for 2–3 h and monitoring *via* TLC until the complete conversion of the reagents. Subsequently, the system was cooled to r.t., and filtered, washed with cold methanol to provide **9a–g** in 70%–75% yield.

4.2.3. General procedure for preparation of 15a–d, 16 and 17

To a solution of **10a–d** (5 mmol) and NaOH (5 mmol) in water (15 mL) was injected compound **13** (5 mmol) dropwise, the mixture was stirred at r.t. for 3–4 h. Subsequently, compound **14** (5 mmol) was added in portions, after stirring for 2 h, hydrazine hydrate (80%, *w/w*, 15 mmol) was added, then the mixture was heated at 65 °C for 2–3 h until a large amount of solids was precipitated, kept stirring for another 0.5 h, then cooled to r.t., and allowed to stand overnight for crystallization to afford compounds **15a–d** with the yield ranging from 40% to 55%. These

intermediates were used for the next step without purification. Likewise, compounds **16** and **17** were derived from reagents **13** and **14** respectively in the same way.

4.2.4. General procedure for preparation of 19a–bf

To the solution of **9a–g** (1.2 mmol) in methanol (5 mL) containing catalytic amount of acetic acid (0.012 mmol), appropriate aldehyde or ketone **18** (1.3 mmol) was added dropwise. The mixture was heated under reflux at 70 °C for 2 h, then cooled to r.t., the precipitation was filtered and recrystallized with methanol, or purified by column chromatography (ethyl acetate/petroleum ether = 1:10) to get compounds **19a–19ad** as solid in 65%–85% yield. Likewise, the rest of target compounds were prepared by reagents **15a–d**, **16** and **17** in the same way. Noteworthy, compounds **19ba–19bc** were not directly derived from the intermediate **15c**, the additional reaction occurred in the solvent of dioxane with conc. HCl as the reagent to remove the Boc protective group.

All the target compounds **19** were synthesized in >95% purity degree. The detailed information on characterization of some representative target compounds were shown below, the rest was summarized in Supporting Information. In addition, the UPLC chromatogram of compounds **19ba** and **19bd** were shown in Supporting Information Figs. S6 and S7.

4.2.4.1. (*E*)-*N*-Phenyl-2-(pyridin-2-ylmethylene)hydrazine-1-carbothioamide (**19e**). White solid, Yield 78%, m.p. 200–201 °C. ^1H NMR (400 MHz, $\text{DMSO}-d_6$, ppm) δ 12.04 (s, 1H, –NH–, D_2O exchangeable), 10.26 (s, 1H, –NH–, D_2O exchangeable), 8.59 (d, J = 4.3 Hz, 1H, Ar–H), 8.45 (d, J = 8.0 Hz, 1H, Ar–H), 8.21 (s, 1H, –CH=N–), 7.85 (td, J = 7.8, 1.3 Hz, 1H, Ar–H), 7.56 (d, J = 7.6 Hz, 2H, Ar–H), 7.42–7.37 (m, 3H, Ar–H), 7.23 (t, J = 7.4 Hz, 1H, Ar–H). ^{13}C NMR (100 MHz, $\text{DMSO}-d_6$, ppm) δ 176.41, 153.15, 149.31, 143.05, 138.94, 136.47, 128.09, 126.07, 125.52, 124.22, 120.60. HR-MS (ESI), Calcd. $\text{C}_{13}\text{H}_{12}\text{N}_4\text{S}$, $[\text{M}+\text{Na}]^+$ m/z : 279.0680, Found: 279.0681.

4.2.4.2. (*E*)-*N*-Phenyl-2-(pyridin-3-ylmethylene)hydrazine-1-carbothioamide (**19f**). White solid, Yield 85%, m.p. 234–235 °C. ^1H NMR (400 MHz, $\text{DMSO}-d_6$, ppm) δ 11.98 (s, 1H, –NH–, D_2O exchangeable), 10.22 (s, 1H, –NH–, D_2O exchangeable), 9.04 (d, J = 1.7 Hz, 1H, Ar–H), 8.59 (dd, J = 4.8, 1.5 Hz, 1H, Ar–H), 8.39 (dt, J = 8.0, 1.7 Hz, 1H, Ar–H), 8.19 (s, 1H, –CH=N–), 7.56 (d, J = 7.7 Hz, 2H, Ar–H), 7.45 (dd, J = 7.9, 4.8 Hz, 1H, Ar–H), 7.38 (t, J = 7.8 Hz, 2H, Ar–H), 7.22 (t, J = 7.4 Hz, 1H, Ar–H). ^{13}C NMR (100 MHz, $\text{DMSO}-d_6$, ppm) δ 176.26, 150.44, 149.05, 139.86, 138.98, 134.17, 130.01, 128.04, 126.04, 125.43, 123.69. HR-MS (ESI), Calcd. $\text{C}_{13}\text{H}_{12}\text{N}_4\text{S}$, $[\text{M}+\text{Na}]^+$ m/z : 279.0680, Found: 279.0681.

4.2.4.3. (*E*)-*N*-Phenyl-2-(pyridin-4-ylmethylene)hydrazine-1-carbothioamide (**19g**). White solid, Yield 78%, m.p. 194–195 °C. ^1H NMR (400 MHz, $\text{DMSO}-d_6$, ppm) δ 12.08 (s, 1H, –NH–, D_2O exchangeable), 10.29 (s, 1H, –NH–, D_2O exchangeable), 8.63 (d, J = 6.0 Hz, 2H, Ar–H), 8.12 (s, 1H, –CH=N–), 7.89 (d, J = 6.0 Hz, 2H, Ar–H), 7.55 (d, J = 7.7 Hz, 2H, Ar–H), 7.39 (t, J = 7.8 Hz, 2H, Ar–H), 7.24 (t, J = 7.4 Hz, 1H, Ar–H). ^{13}C NMR (100 MHz, $\text{DMSO}-d_6$, ppm) δ 176.58, 150.00, 141.26, 140.00, 138.90, 128.11, 126.17, 125.61,

121.36. HR-MS (ESI), Calcd. $C_{13}H_{12}N_4S$, $[M+Na]^+$ m/z : 279.0680, Found: 279.0682.

4.2.4.4. (*E*)-*N*-(4-Bromophenyl)-2-(pyridin-2-ylmethylene)hydrazine-1-carbothioamide (**19m**). White solid, Yield 65%, m.p. 225–226 °C. 1H NMR (400 MHz, DMSO- d_6 , ppm) δ 12.12 (s, 1H, –NH–, D₂O exchangeable), 10.28 (s, 1H, –NH–, D₂O exchangeable), 8.59 (d, J = 4.3 Hz, 1H, Ar–H), 8.43 (d, J = 8.0 Hz, 1H, Ar–H), 8.21 (s, 1H, –CH=N–), 7.86 (td, J = 7.7, 1.3 Hz, 1H, Ar–H), 7.60–7.54 (m, 4H, Ar–H), 7.43–7.38 (m, 1H, Ar–H). ^{13}C NMR (100 MHz, DMSO- d_6 , ppm) δ 176.33, 153.04, 149.36, 143.41, 138.36, 136.48, 130.92, 127.97, 124.30, 120.63, 117.78. HR-MS (ESI), Calcd. $C_{13}H_{11}BrN_4S$, $[M+Na]^+$ m/z : 356.9785, Found: 356.9785.

4.2.4.5. (*E*)-*N*-(2-Bromophenyl)-2-(1-(pyridin-2-yl)ethylidene)hydrazine-1-carbothioamide (**19r**). White solid, Yield 73%, m.p. 161–162 °C. 1H NMR (400 MHz, DMSO- d_6 , ppm) δ 10.93 (s, 1H, –NH–, D₂O exchangeable), 10.19 (s, 1H, –NH–, D₂O exchangeable), 8.64–8.58 (m, 1H, Ar–H), 8.52 (d, J = 8.1 Hz, 1H, Ar–H), 7.86–7.78 (m, 1H, Ar–H), 7.74 (ddd, J = 11.8, 8.0, 1.4 Hz, 2H, Ar–H), 7.47–7.38 (m, 2H, Ar–H), 7.25 (td, J = 7.8, 1.6 Hz, 1H, Ar–H), 2.48 (s, 3H, –CH₃). ^{13}C NMR (100 MHz, DMSO- d_6 , ppm) δ 177.59, 154.46, 149.16, 148.50, 137.94, 136.45, 132.38, 129.73, 128.04, 127.70, 124.13, 121.36, 121.03, 12.52. HR-MS (ESI), Calcd. $C_{14}H_{13}BrN_4S$, $[M+Na]^+$ m/z : 370.9942, Found: 370.9942.

4.2.4.6. (*E*)-*N*-Phenyl-2-(1-(pyridin-2-yl)ethylidene)hydrazine-1-carbothioamide (**19ac**). Yellow solid, Yield 76%, m.p. 192–193 °C. 1H NMR (400 MHz, DMSO- d_6 , ppm) δ 10.67 (s, 1H, –NH–, D₂O exchangeable), 10.19 (s, 1H, –NH–, D₂O exchangeable), 8.61 (dd, J = 4.8, 0.7 Hz, 1H, Ar–H), 8.54 (d, J = 8.1 Hz, 1H, Ar–H), 7.82 (td, J = 8.0, 1.7 Hz, 1H, Ar–H), 7.56 (d, J = 7.6 Hz, 2H, Ar–H), 7.40 (dt, J = 14.2, 4.5 Hz, 3H, Ar–H), 7.23 (t, J = 7.4 Hz, 1H, Ar–H), 2.47 (s, 3H, –CH₃). ^{13}C NMR (100 MHz, DMSO- d_6 , ppm) δ 177.24, 154.50, 149.17, 148.45, 139.12, 136.35, 128.08, 126.11, 125.52, 124.08, 121.21, 12.46. HR-MS (ESI), Calcd. $C_{14}H_{14}N_4S$, $[M+H]^+$ m/z : 271.1017, Found: 271.1016.

4.2.4.7. (*E*)-*N'*-(2-Hydroxybenzylidene)benzohydrazide (**19ae**). Yellow solid, Yield 77%, m.p. 172–173 °C. 1H NMR (400 MHz, DMSO- d_6 , ppm) δ 12.14 (s, 1H, –OH, D₂O exchangeable), 11.32 (s, 1H, –NH–, D₂O exchangeable), 8.66 (s, 1H, –CH=N–), 7.96 (d, J = 7.4 Hz, 2H, Ar–H), 7.63 (t, J = 7.2 Hz, 1H, Ar–H), 7.56 (t, J = 7.1 Hz, 3H, Ar–H), 7.32 (t, J = 7.7 Hz, 1H, Ar–H), 7.00–6.89 (m, 2H, Ar–H). ^{13}C NMR (100 MHz, DMSO- d_6 , ppm) δ 162.79, 157.43, 148.20, 132.76, 131.98, 131.38, 129.47, 128.54, 127.62, 119.33, 118.65, 116.39. HR-MS (ESI), Calcd. $C_{14}H_{12}N_2O_2$, $[M+H]^+$ m/z : 241.0977, Found: 241.0970.

4.2.4.8. (*E*)-*N'*-(1-(5-Chloro-2-hydroxyphenyl)ethylidene)benzohydrazide (**19af**). Yellow solid, Yield 79%, m.p. 206–207 °C. 1H NMR (400 MHz, DMSO- d_6 , ppm) δ 13.46 (s, 1H, –OH, D₂O exchangeable), 11.45 (s, 1H, –NH–, D₂O exchangeable), 7.96 (s, 1H, Ar–H), 7.94 (s, 1H, Ar–H), 7.68–7.61 (m, 2H, Ar–H), 7.55 (t, J = 7.5 Hz, 2H, Ar–H), 7.34 (d, J = 8.7 Hz, 1H, Ar–H), 6.95 (d, J = 8.7 Hz, 1H, Ar–H), 2.50 (s, 3H, –CH₃). ^{13}C NMR

(100 MHz, DMSO- d_6 , ppm) δ 164.51, 157.42, 156.62, 132.72, 132.08, 130.75, 128.41, 128.18, 127.74, 122.07, 120.81, 119.08, 14.16. HR-MS (ESI), Calcd. $C_{15}H_{13}ClN_2O_2$, $[M+H]^+$ m/z : 289.0744, Found: 289.0738.

4.2.4.9. (*E*)-*N'*-(1-(Pyridin-2-yl)ethylidene)morpholine-4-carbothiohydrazide (**19ag**). Yellow solid, Yield 75%, m.p. 213–215 °C. 1H NMR (400 MHz, DMSO- d_6 , ppm) δ 9.96 (s, 1H, –NH–, D₂O exchangeable), 8.67 (d, J = 52.9 Hz, 1H, Ar–H), 8.11–7.80 (m, 2H, Ar–H), 7.47 (d, J = 47.2 Hz, 1H, Ar–H), 3.95 (s, 4H, –CH₂CH₂–), 3.65 (s, 4H, –CH₂CH₂–), 2.40 (s, 3H, –CH₃). ^{13}C NMR (101 MHz, CDCl₃, ppm) δ 188.17, 186.70, 136.24, 133.63, 123.76, 122.36, 71.03, 70.91, 54.00, 52.98. HR-MS (ESI), Calcd. $C_{12}H_{17}N_4OS$, $[M+H]^+$ m/z : 265.1123, Found: 265.1122.

4.2.4.10. (*E*)-*N'*-(Pyridin-2-ylmethylene)piperidine-1-carbothiohydrazide (**19ai**). Brown solid, Yield 75%, m.p. 213–215 °C. 1H NMR (400 MHz, DMSO- d_6 , ppm) δ 11.25 (s, 1H, –NH–, D₂O exchangeable), 8.58 (d, J = 4.9 Hz, 1H, Ar–H), 8.17 (s, 1H, –CH=N–), 7.84 (d, J = 4.2 Hz, 2H, Ar–H), 7.37 (q, J = 4.5 Hz, 1H, Ar–H), 3.88 (t, J = 4.9 Hz, 4H, –CH₂–), 1.74–1.46 (m, 6H, –CH₂CH₂CH₂–). ^{13}C NMR (101 MHz, DMSO- d_6 , ppm) δ 180.15, 153.47, 149.41, 143.35, 136.71, 123.85, 119.27, 51.23, 25.75, 23.85. HR-MS (ESI), Calcd. $C_{12}H_{16}N_4S$, $[M+H]^+$ m/z : 249.1174, Found: 249.1167.

4.2.4.11. (*E*)-*N*-Cyclohexyl-2-(1-(pyridin-2-yl)ethylidene)hydrazine-1-carbothioamide (**19aj**). Yellow solid, Yield 75%, m.p. 171–172 °C. 1H NMR (400 MHz, DMSO- d_6 , ppm) δ 10.26 (s, 1H, –NH–, D₂O exchangeable), 8.59 (d, J = 4.7 Hz, 1H, –NH–, D₂O exchangeable), 8.29 (d, J = 8.1 Hz, 1H, Ar–H), 8.14 (d, J = 8.5 Hz, 1H, Ar–H), 7.84 (td, J = 7.8, 1.7 Hz, 1H, Ar–H), 7.44–7.33 (m, 1H, Ar–H), 4.29–4.15 (m, 1H, –CH), 2.40 (s, 3H, –CH₃), 1.94–1.86 (m, 2H, –CH₂–), 1.74 (d, J = 12.9 Hz, 2H, –CH₂–), 1.62 (d, J = 12.5 Hz, 1H, –CH₂–), 1.47 (qd, J = 12.2, 3.1 Hz, 2H, –CH₂–), 1.37–1.24 (m, 2H, –CH₂–), 1.22–1.10 (m, 1H, –CH₂–). ^{13}C NMR (100 MHz, DMSO- d_6 , ppm) δ 176.72, 154.62, 148.50, 148.25, 136.44, 123.92, 120.69, 52.81, 31.59, 25.10, 24.84, 12.26. HR-MS (ESI), Calcd. $C_{14}H_{20}N_4S$, $[M+Na]^+$ m/z : 299.1306, Found: 299.1308.

4.2.4.12. (*E*)-*N,N*-Dimethyl-2-(1-(pyridin-2-yl)ethylidene)hydrazine-1-carbothioamide (**19ak**). Yellow solid, Yield 75%, m.p. 195–196 °C. 1H NMR (400 MHz, DMSO- d_6 , ppm) δ 9.60 (s, 1H, –NH–, D₂O exchangeable), 8.59 (s, 1H, Ar–H), 7.89–7.77 (m, 2H, Ar–H), 7.39 (s, 1H, Ar–H), 3.32 (s, 6H, –CH₃), 2.40 (s, 3H, –CH₃). ^{13}C NMR (101 MHz, DMSO- d_6 , ppm) δ 179.92, 152.20, 147.43, 138.67, 124.34, 124.19, 120.02, 42.18, 21.87. HR-MS (ESI), Calcd. $C_{10}H_{14}N_4S$, $[M+H]^+$ m/z : 223.1017, Found: 223.1015.

4.2.4.13. (*E*)-*N'*-(Pyridin-2-ylmethylene)morpholine-4-carbothiohydrazide (**19ao**). White solid, Yield 77%, m.p. 201–203 °C. 1H NMR (400 MHz, DMSO- d_6 , ppm) δ 11.44 (s, 1H, –NH–, D₂O exchangeable), 8.58 (dd, J = 4.8, 1.5 Hz, 1H, Ar–H), 8.18 (s, 1H, –CH=N–), 7.85 (dt, J = 3.4, 1.5 Hz, 2H, Ar–H), 7.38 (td, J = 5.2, 3.0 Hz, 1H, Ar–H), 3.94 (t, J = 4.8 Hz, 4H, –CH₂CH₂–), 3.76–3.62 (m, 4H, –CH₂CH₂–). ^{13}C NMR (101 MHz, DMSO- d_6 , ppm) δ 180.83, 153.26, 149.43, 144.04,

136.77, 124.02, 119.47, 65.97, 50.58. HR-MS (ESI), Calcd. $C_{11}H_{14}N_4OS$, $[M+H]^+$ m/z : 251.0967, Found: 251.0967.

4.2.4.14. (*E*)-*N'*-(4-Bromobenzylidene)morpholine-4-carbothiohydrazide (**19ap**). Yellow solid, Yield 80%, m.p. 169–170 °C. 1H NMR (400 MHz, DMSO- d_6 , ppm) δ 11.27 (s, 1H, –NH–, D₂O exchangeable), 8.12 (s, 1H, –CH=N–), 7.66–7.53 (m, 4H, Ar–H), 3.93–3.89 (m, 4H, –CH₂CH₂–), 3.70–3.65 (m, 4H, –CH₂CH₂–). ^{13}C NMR (100 MHz, DMSO- d_6 , ppm) δ 180.75, 142.66, 133.58, 131.82, 128.61, 122.87, 65.98, 50.47. HR-MS (ESI), Calcd. $C_{12}H_{14}BrN_3OS$, $[M+H]^+$ m/z : 330.0099, Found: 330.0090.

4.2.4.15. (*E*)-*N'*-((1*H*-Indol-3-yl)methylene)morpholine-4-carbothiohydrazide (**19ar**). Yellow solid, Yield 77%, m.p. 165–166 °C. 1H NMR (400 MHz, DMSO- d_6 , ppm) δ 11.57 (s, 1H, –NH–, D₂O exchangeable), 10.98 (s, 1H, –NH–, D₂O exchangeable), 8.36 (s, 1H, –CH=N–), 8.17 (d, J = 7.6 Hz, 1H, Ar–H), 7.78 (d, J = 2.7 Hz, 1H, Ar–H), 7.43 (d, J = 7.9 Hz, 1H, Ar–H), 7.22–7.11 (m, 2H, Ar–H), 3.96–3.93 (m, 4H, –CH₂CH₂–), 3.72–3.68 (m, 4H, –CH₂CH₂–). ^{13}C NMR (100 MHz, DMSO- d_6 , ppm) δ 180.34, 141.91, 137.02, 130.38, 124.03, 122.57, 121.76, 120.48, 111.80, 111.45, 66.03, 50.17. HR-MS (ESI), Calcd. $C_{14}H_{16}N_4OS$, $[M-H]^-$ m/z : 287.0967, Found: 287.0966.

4.2.4.16. (*E*)-*N'*-((5-Bromopyridin-2-yl)methylene)morpholine-4-carbothiohydrazide (**19as**). Yellow solid, Yield 80%, m.p. 205–206 °C. 1H NMR (400 MHz, DMSO- d_6 , ppm) δ 11.49 (s, 1H, –NH–, D₂O exchangeable), 8.71 (d, J = 2.3 Hz, 1H, Ar–H), 8.15 (s, 1H, –CH=N–), 8.09 (dd, J = 8.6, 2.3 Hz, 1H, Ar–H), 7.80 (d, J = 8.6 Hz, 1H, Ar–H), 3.93 (t, J = 4.7 Hz, 4H, –CH₂CH₂–), 3.68 (t, J = 4.7 Hz, 4H, –CH₂CH₂–). ^{13}C NMR (101 MHz, DMSO- d_6 , ppm) δ 180.76, 152.13, 150.13, 142.83, 139.46, 121.03, 120.29, 65.94, 50.51. HR-MS (ESI), Calcd. $C_{11}H_{13}BrN_4OS$, $[M+H]^+$ m/z : 329.0072, Found: 329.0064.

4.2.4.17. (*E*)-*N'*-(2-Hydroxybenzylidene)piperazine-1-carbothiohydrazide (**19ba**). Yellow solid, Yield 75%, m.p. 215–216 °C. 1H NMR (400 MHz, DMSO- d_6 , ppm) δ 12.12 (s, 1H, –NH–, D₂O exchangeable), 8.41 (s, 1H, –CH=N–), 7.35 (dd, J = 7.9, 1.8 Hz, 1H, Ar–H), 7.23 (td, J = 7.7, 1.7 Hz, 1H, Ar–H), 6.86 (dd, J = 7.8, 5.8 Hz, 2H, Ar–H), 3.89 (dd, J = 6.1, 3.9 Hz, 4H, –CH₂CH₂–), 2.88–2.71 (m, 4H, –CH₂CH₂–). ^{13}C NMR (101 MHz, DMSO- d_6 , ppm) δ 179.84, 157.28, 145.79, 130.22, 129.67, 118.86, 118.70, 116.37, 48.78, 44.97. HR-MS (ESI), Calcd. $C_{12}H_{16}N_4OS$, $[M+H]^+$ m/z : 265.1123, Found: 265.1116.

4.2.4.18. (*E*)-*N'*-(2-Methoxybenzylidene)piperazine-1-carbothiohydrazide (**19bb**). Yellow solid, Yield 81%, m.p. 204–205 °C. 1H NMR (400 MHz, DMSO- d_6 , ppm) δ 8.54 (s, 1H, –CH=N–), 7.75 (dd, J = 7.8, 1.7 Hz, 1H, Ar–H), 7.45–7.36 (m, 1H, Ar–H), 7.10 (d, J = 8.4 Hz, 1H, Ar–H), 7.01 (t, J = 7.5 Hz, 1H, Ar–H), 4.09 (t, J = 5.0 Hz, 4H, –CH₂CH₂–), 3.86 (s, 3H, –CH₃), 3.33–3.02 (m, 4H, –CH₂CH₂–). ^{13}C NMR (101 MHz, DMSO- d_6 , ppm) δ 181.08, 157.66, 140.33, 131.45, 120.73, 111.84, 55.72, 47.05, 42.93. HR-MS (ESI), Calcd. $C_{13}H_{18}N_4OS$, $[M+H]^+$ m/z : 279.1280, Found: 279.1269.

4.2.4.19. (*E*)-*N'*-(2-Ethoxybenzylidene)piperazine-1-carbothiohydrazide (**19bc**). Yellow solid, Yield 83%, m.p.

209–210 °C. 1H NMR (400 MHz, DMSO- d_6 , ppm) δ 11.13 (s, 1H, –NH–, D₂O exchangeable), 8.52 (s, 1H, –CH=N–), 7.74 (d, J = 7.7 Hz, 1H, Ar–H), 7.36 (t, J = 8.0 Hz, 1H, Ar–H), 7.07 (d, J = 8.4 Hz, 1H, Ar–H), 6.98 (t, J = 7.5 Hz, 1H, Ar–H), 4.11 (q, J = 6.9 Hz, 2H, –CH₂–), 3.86 (t, J = 4.8 Hz, 4H, –CH₂CH₂–), 2.82 (t, J = 4.9 Hz, 4H, –CH₂CH₂–), 1.38 (t, J = 6.9 Hz, 3H, –CH₃). ^{13}C NMR (101 MHz, DMSO- d_6 , ppm) δ 157.06, 140.62, 120.69, 112.84, 43.03, 42.67, 21.06, 14.63. HR-MS (ESI), Calcd. $C_{14}H_{20}N_4OS$, $[M+H]^+$ m/z : 293.1436, Found: 293.1426.

4.2.4.20. (*E*)-*N'*-(2-Hydroxybenzylidene)-4-methylpiperazine-1-carbothiohydrazide (**19bd**). Yellow solid, Yield 82%, m.p. 176–177 °C. 1H NMR (400 MHz, DMSO- d_6 , ppm) δ 11.59 (s, 1H, –NH–, D₂O exchangeable), 8.46 (s, 1H, –CH=N–), 7.41 (dd, J = 7.9, 1.5 Hz, 1H, Ar–H), 7.30–7.23 (m, 1H, Ar–H), 6.93–6.87 (m, 2H, Ar–H), 4.01–3.74 (m, 4H, –CH₂CH₂–), 2.43–2.38 (m, 4H, –CH₂CH₂–), 2.23 (s, 3H, –CH₃). ^{13}C NMR (100 MHz, DMSO- d_6 , ppm) δ 171.98, 157.05, 146.13, 130.82, 129.92, 119.04, 118.47, 116.49, 54.14, 48.25, 45.26, 21.03. HR-MS (ESI), Calcd. $C_{13}H_{18}N_4OS$, $[M+H]^+$ m/z : 279.1280, Found: 279.1278.

4.2.4.21. (*E*)-*N'*-(2-Methoxybenzylidene)-4-methylpiperazine-1-carbothiohydrazide (**19be**). Yellow solid, Yield 85%, m.p. 178–179 °C. 1H NMR (400 MHz, DMSO- d_6 , ppm) δ 11.16 (s, 1H, –NH–, D₂O exchangeable), 8.49 (s, 1H, –CH=N–), 7.74 (d, J = 7.7 Hz, 1H, Ar–H), 7.39 (t, J = 8.0 Hz, 1H, Ar–H), 7.09 (d, J = 8.4 Hz, 1H, Ar–H), 7.00 (t, J = 7.6 Hz, 1H, Ar–H), 3.89 (t, J = 4.9 Hz, 4H, –CH₂CH₂–), 3.84 (s, 3H, –CH₃), 2.39 (t, J = 4.9 Hz, 4H, –CH₂CH₂–), 2.21 (s, 3H, –CH₃). ^{13}C NMR (101 MHz, DMSO- d_6 , ppm) δ 180.43, 157.53, 139.49, 131.11, 125.21, 122.39, 120.71, 111.79, 55.65, 54.42, 49.65, 45.38. HR-MS (ESI), Calcd. $C_{14}H_{20}N_4OS$, $[M+H]^+$ m/z : 293.1436, Found: 293.1427.

4.2.4.22. (*E*)-*N'*-(2-Ethoxybenzylidene)-4-methylpiperazine-1-carbothiohydrazide (**19bf**). Yellow solid, Yield 78%, m.p. 182–183 °C. 1H NMR (400 MHz, DMSO- d_6 , ppm) δ 11.18 (s, 1H, –NH–, D₂O exchangeable), 8.52 (s, 1H, –CH=N–), 7.74 (d, J = 7.7 Hz, 1H, Ar–H), 7.36 (t, J = 8.0 Hz, 1H, Ar–H), 7.06 (d, J = 8.4 Hz, 1H, Ar–H), 6.98 (t, J = 7.6 Hz, 1H, Ar–H), 4.10 (q, J = 6.9 Hz, 2H, –CH₂–), 3.89 (t, J = 4.8 Hz, 4H, –CH₂CH₂–), 2.40 (t, J = 4.9 Hz, 4H, –CH₂CH₂–), 2.21 (s, 3H, –CH₃), 1.37 (t, J = 7.0 Hz, 3H, –CH₃). ^{13}C NMR (101 MHz, DMSO- d_6 , ppm) δ 180.49, 156.94, 139.73, 131.06, 125.20, 122.64, 120.66, 112.83, 63.82, 54.43, 49.67, 45.38, 14.64. HR-MS (ESI), Calcd. $C_{15}H_{22}N_4OS$, $[M+H]^+$ m/z : 307.1593, Found: 307.1588.

4.3. Biological

4.3.1. Standard agar disk diffusion assay

Standard operation was performed according to CLSI M07-A9 guidelines. *E. coli* ATCC 25922 (American Type Culture Collection, Maryland, USA) was used as control. DMSO (Tianjing Hengxing Chemical Reagent Co., Ltd., Tianjin, China) was used as a solution. After 6 h of culture, 10^9 CFU/mL strains were taken and diluted to 10^5 CFU/mL with Mueller-Hinton Broth (MHB, Beijing Aoboxing Biotechnology Co., Ltd., Beijing, China). The bacterial solution was evenly coated on Mueller-Hinton Agar (MHA, Beijing Aoboxing Biotechnology Co., Ltd.) plate. MEM/MEM-EDTA or test paper was analyzed by agar disc diffusion method with or without 0.5 mol/L EDTA (Beijing Solarbio Science and Technology Co., Ltd., Beijing, China)/test material.

After 16–18 h, the bacteriostatic circle was cultured at 37 °C. The results were in accordance with the CLSI standard.

4.3.2. Minimum inhibitory concentration (MIC) assay

According to the regulations of CLSI, broth microdilution method was used to evaluate the antimicrobial activity. Bacteria were cultured in MHB to 10^9 CFU/mL. After diluting it 1000 times, bacteria with a concentration of about 10^6 CFU/mL was obtained. The compounds were dissolved in water and diluted with MHB. MEM was gradient diluted to 0.3125–16 mg/mL. The diluted MHB drug (256 or 128 µg/mL) and the diluted bacterial culture medium (10^6 CFU/mL) was added to 96-well plate. The final volume of each hole in 96-well plate was 200 µL. The concentration of other compounds in 96-well plate was 4 times as high as that in bacterial culture medium, except that the dilution of bacterial culture medium was 2 times as 5×10^5 CFU/mL. The plate was incubated at 37 °C for 16–18 h. In addition to the blank control group (medium only), the positive control group (containing only bacterial solution) was set up in all experiments. The MIC of the tested drug showed no bacterial growth in the tube at the lowest concentration. The reported experimental results were the average of three independent experiments.

4.3.3. Metal suppression experiments

Zinc homeostasis testing experiment was carried out according to the MIC of the combination drug. Zn^{2+} plays a major role in MBL. Therefore, we designed a Zn^{2+} metal ion inhibition experiment to test the sensitivity of the compound to MEM in the presence of Zn^{2+} ions. The concentration of monotherapy treatment groups of MEM = 2 µg/mL, EDTA = 32 µg/mL, compound **19bg** = 32 µg/mL and compound **19bh** = 32 µg/mL. The operation was the same except that an equimolar amount of $ZnCl_2$ (32 µg/mL, Heowns Biochem Technologies LLC., Tianjin, China) was added. Incubated at 37 °C for 1 h and measured the absorbance at OD = 600 nm. Results were plotted as mean \pm SD of three samples.

4.3.4. Haemolytic activity

Preparation of 5% red blood cell suspension: fresh sterile sheep blood (Bianzhen Biotechnology Co., Ltd., Nanjing, China) was suspended in sterile $1 \times$ PBS buffer (Beijing Solarbio Science and Technology Co., Ltd.) and diluted by centrifugation ($1500 \times g$, 10 min). In the experiment, a hemolysis assay was carried out using water as a solvent (final concentration not exceeding 0.5%) to prevent false positive results, and 0.1% Triton-X detergent (Beijing Solarbio Science and Technology Co., Ltd.) was used as a positive control⁴⁴. A 150 µL/well 5% red blood cell suspension was pipetted into a 96-well plate. The drug was diluted in $1 \times$ PBS buffer, 50 µL per well, and three parallel wells were made at the same concentration. After incubating for 1 h in a 37 °C incubator, the plates were placed in a centrifuge (3500 rpm, 5 min, TDZ5-WS, Xiangyi Laboratory Instrument Development Co., Ltd., Changsha, China). Transfer 100 µL/well of supernatant to a new 96-well plate. Finally, the results were measured at 540 nm on a microplate reader (318MC, Boteng Instrument Equipment Co., Ltd., Shenyang, China). The percentage of hemolysis was determined as Eq. (1):

$$\text{Hemolysis (\%)} = (A - A_0)/(A_{\text{Total}} - A_0) \times 100 \quad (1)$$

where A was the test well, A_0 was the negative control, and A_{Total} was positive control.

4.3.5. CCK-8 and EdU cell proliferation assay

Target HeLa cells (Thermo Fisher scientific, Waltham, MA, USA) were diluted into 5×10^4 cells/mL with the medium, 100 µL of the cell suspension was seeded in each well of 96-well cell culture plates and incubated in the presence of different concentrations of compounds **19bg** and **19bh** at 37 °C for 48 h. Cells proliferation was detected with CCK-8 cell counting kit (vazyme, A311-01, Nanjing, China), and the protocol was followed according to the manufacturer's instructions. All measurements were performed in triplicate. DNA synthesis in living cells was detected by using the EdU cell proliferation assay Kit (Beyotime, C0075S, Shanghai, China), and the protocol was followed according to the manufacturer's instructions. The EdU fluorescence was observed under an Olympus laser scanning confocal microscope (Leica microsystems, Shanghai, China).

4.3.6. Enzyme inhibition

The final concentrations of NDM-1 inhibitor compounds **19bg** and **19bh** were set to 20, 10, 5, 2.5, 1.25, 0.625, 0.3125 and 0 µg/mL in a 200 µL enzyme reaction system; three parallel control groups were set up on a 96-well UV plate according to the corresponding concentration dilution gradient. Dilute the NDM-1 enzyme solution in 10 mmol/L HEPES buffer, add 98 µL of the diluted enzyme solution and two µL of the screening sample to each well, incubate at 30 °C for 15 min; then 100 µL of the diluted substrate solution was added to each well to initiate the reaction with end concentration of 250 µmol/L; the 96-well UV plate was placed in the Multimode Plate Reader (EnSpire, PerkinElmer, Waltham, MA, USA). It was measured at intervals of 1 min at 30 °C for a total of 60 min. The absorbance at OD₃₀₀ was measured. The inhibition rate of the enzyme was calculated. The IC₅₀ of each inhibitor was analyzed using GraphPad Prism version 5.0 (GraphPad Software, San Diego, CA, USA).

4.3.7. Expression and purification of NDM-1 enzyme

The $bla_{\text{NDM-1}}$ sequence that encoding N-terminus truncated protein (residue G29–R270) was amplified by PCR (Life technologies, QuantStudio 6 Flex, Thermo Fisher scientific, MA, USA) and purified $bla_{\text{NDM-1}}$ PCR product was cloned into the pET28a vector between NdeI and XhoI restriction site. The recombinant plasmid was sequenced and introduced into *E. coli* BL21 (DE3) for expressing. *E. coli* BL21 (DE3)/pET-28a-NDM-1 was induced by 0.5 mmol/L IPTG, 20 °C, to cultivate 16 h. After induction, bacterial cells were collected and sonicated. The system was purified by using His Trap Q 5-mL column (GE healthcare, Boston, USA) as a purification medium, and the buffer was 250 mmol/L imidazole-containing PBS solution (pH 7.5) to obtain a higher purity recombinant protein solution. At last purified NDM-1 was stored in the buffer (150 mmol/L NaCl, 2 mmol/L $ZnCl_2$, 20 mmol/L Tris, pH 7.5) and frozen at -80 °C until further use.

4.3.8. K_i measurement method

A 200 µL NDM-1 enzyme reaction system (2 µL inhibitor, 98 µL NDM-1 enzyme and 100 µL MEM) was selected with final concentrations of inhibitors of 0, 2.5, and 5.0 mg/mL. The NDM-1 enzyme was diluted with 10 mmol/L HEPES, the inhibitor was diluted with water to the set concentration gradient, and the sample was incubated at 30 °C for 15 min. For different concentrations of compound, the substrate concentration was varied and the final concentrations of substrate MEM were 8.25, 6.25, 12.5, 25, 50, 100, 200 and 400 mmol/L. After measuring the absorbance in the OD₃₀₀ using a microplate reader (318MC, Boteng Instrument Equipment

Co., Ltd., Shenyang, China), the measurement was continued for 60 min and measured every 1 min. Finally, the reaction rates of each compound concentration were calculated separately, and the Lineweaver-Burke curve at different compound concentrations, the double reciprocal curve of the reaction rate and the substrate concentration were calculated. The K_i value was calculated using GraphPad prism software to analyze the type of inhibition of the NDM-1 enzyme by the compound.

4.3.9. Time-dependent killing assay

The strains (A total of 10 NDM-1 positive non-duplicate *K. pneumoniae* isolates, which were obtained from a teaching hospital of Zhengzhou University, Zhengzhou, China) were grown overnight (incubated at 37 °C with aeration at 225 rpm) with Shaker (ZWY-1102C, Zhicheng Analytical Instrument Manufacturing Co., Ltd., Shanghai, China). On the next day, the bacterial solution was diluted 1:10,000 with MHB medium, and placed on a constant temperature shaker at 37 °C for 225 rpm to continue growth for 2 h, after which different concentrations of MIC compounds and meropenem were added. At this time, it was 0 h, 100 μ L of the sample solution was taken out from the EP tube, centrifuged at 10,000 \times *g* in a centrifuge, the supernatant was discarded, and a sterile 96-well plate was taken and diluted with 1 \times PBS buffer. Diluted 10 times in sequence, and took 10 μ L of the sample droplet from the diluted well and added it to the MHA solid medium to mark it. This was the colony count at 0 h. At this time, according to the above sampling method, the colony counts were performed for 1, 2, 3, to 24 h, and the time sterilization curve was obtained with Origin version 8.0 (OriginLab, Northampton, MA, USA). The bacterial colonies were counted and results represented in log₁₀ (CFU/mL) using the origin 8.0. And photos the bacteria control for 24 h.

4.3.10. In vivo sepsis animal experiment

Animals experiment was carried out according to the approved guidelines of the Institutional Animal Care and Use Committee. Female BALB/c nude mice weighing 15–18 g and aged 7–9 weeks were purchased from Henan Hua Xing of Laboratory Animal Co., Ltd. (HXDW20010004, Zhengzhou, China). Drug safety evaluation experiment was to examine the safety of the compound by tissue staining. Experimental mice were randomized to cages of two per group for this experiment. The mice were divided into three groups: NS (normal saline, subcutaneous injection), **19bg** (64 mg/kg, subcutaneous injection) and compound **19bh** (64 mg/kg, subcutaneous injection). Twenty-four hours after injection, all of the mice were euthanized, and these mice were dissected, and liver, spleen and kidney tissues were sectioned and H&E stained. We established murine sepsis models to verify that compounds **19bg** and **19bh** could reverse the resistance of clinical strains of NDM-1 enzyme to MEM. Mice were randomized to cages of 6 per group for this experiment. For all organ bacterial load experiments, BALB/c mice were given a median lethal dose (5×10^6 CFU) of *K. pneumoniae* by i.p. injection and after 30 min post-infection treated with a single dose of MEM (10 mg/kg) and combination of MEM (10 mg/kg) plus compound **19bg** (10 mg/kg), compound **19bh** (10 mg/kg) or PBS by subcutaneous injection. Mice were euthanized 48 h post-infection and treatment, and spleen, liver and kidney were collected. Organs were placed into one mL sterile PBS on ice, and then homogenized. Organ homogenates were then serially diluted in PBS, and selected plating for CFU enumeration. At the same time, H&E staining was used for observing whether liver, spleen and kidney tissue lesions. For survival experiments, BALB/c mice were given a lethal dose of *K. pneumoniae* (1×10^7 CFU) by i.p.

injection and after 30 min post-infection treated with a single dose of MEM (10 mg/kg), compound **19bg** alone (30 mg/kg), compound **19bh** alone (30 mg/kg) and combination of MEM (10 mg/kg) plus compound **19bg** (30 mg/kg) or compound **19bh** (30 mg/kg), or PBS by subcutaneous injection. Mice were monitored for endpoint until 96 h post-infection and treatment.

4.4. Molecular docking assay

To predict the binding mode of uncompetitive inhibitors with NDM-1, we used CavityPlus³⁹ (<http://www.pkumdl.cn/cavityplus>) for molecular docking studies. The X-ray structure of NDM-1 with a hydrolyzed meropenem ligand (PDB ID: 5N0H) was selected for docking. Eleven binding sites were identified by using the Cavity Module with default parameters. The location, max p*K*_d and average p*K*_d value of every binding sites were shown in Supporting Information Fig. S5 and Table S4). Then, cavity one was selected as *ortho*-site (hydrolyzed meropenem ligand binds at cavity 1), CorrSite Module with default parameters of CavityPlus was used to identify potential allosteric binding site. The results outputted 4 allosteric binding sites with a Z-score larger than 0.5 (Supporting Information Table S5).

Compound **19bh** was docked into allosteric binding sites (cavities 4, 2, 7 and 10) respectively using Glide Docking Module of Schrödinger (Version 6.7, Schrodinger, New York, NY, USA) and without hydrolyzed meropenem ligand in the substrate binding site (cavity 1). The docking scores were shown in Supporting Information Table S6. When **19bh** was docked to cavity 7, it formed two H-bond interactions with D95 and Q123. Because H122 and D124 were critical residues for NDM-1-catalyzed carbapenem hydrolysis, we speculated that compound **19bh** was most likely to bind in cavity 7 which was adjacent to the substrate binding site. When we docked **19bh** into cavity 7 with hydrolyzed meropenem ligand in the substrate binding site (cavity 1), there was little change in values. The docking results showed that **19bh** formed two H-bond interactions with D95 and Q123, just like the docking results when hydrolyzed meropenem ligand in the substrate binding site. In addition, compound **19bg** showed a similar binding pattern to compound **19bh**.

Acknowledgments

This work was supported by National Natural Science Foundation of China (Grant Nos. 81903447 for Bing Zhao, 81903623 for Yongfang Yao, 81703328 for Liying Ma, and 81430085 for Hongmin Liu); National Key Research and Development Project of China (Nos. 2016YFA0501800 and 2018YFE0195100 for Hongmin Liu). We thank Prof. Luhua Lai, Dr. Hao Liang and Dr. Wei Yang from Peking University (Beijing, China) for assistance of molecular docking.

Author contributions

Dequan Yu, Hongmin Liu, Liying Ma, and Shangshang Qin were responsible for the conception and design of this work, Bing Zhao, Xinhui Zhang analyzed the literatures, designed and synthesized the compounds, summarized the results and drafted the manuscript. Tingting Yu, Ying Liu, Yongfang Yao and Xuejian Feng did activity test and animal studies. Xiaoling Zhang did docking studies. All authors have read and approved the final manuscript.

Conflicts of interest

The authors have no conflicts of interest to declare.

Appendix A. Supporting information

Supporting data to this article can be found online at <https://doi.org/10.1016/j.apsb.2020.07.005>.

References

- Hutchings MI, Truman AW, Wilkinson B. Antibiotics: past, present and future. *Curr Opin Microbiol* 2019;**51**:72–80.
- Mendelson M, Matsoso MP. The world health organization global action plan for antimicrobial resistance. *S Afr Med J* 2015;**105**:325.
- Bush K, Jacoby GA. Updated functional classification of β -lactamases. *Antimicrob Agents Chemother* 2010;**54**:969–76.
- Bebrone C. Metallo- β -lactamases (classification, activity, genetic organization, structure, zinc coordination) and their superfamily. *Biochem Pharmacol* 2007;**74**:1686–701.
- Hall BG, Barlow M. Revised ambler classification of β -lactamases. *J Antimicrob Chemother* 2005;**55**:1050–1.
- Ambler RP. The structure of β -lactamases. *Philos Trans R Soc Lond B Biol Sci* 1980;**289**:321–31.
- Palzkill T. Metallo- β -lactamase structure and function. *Ann N Y Acad Sci* 2013;**1277**:91–104.
- Yong D, Toleman MA, Giske CG, Cho HS, Sundman K, Lee K, et al. Characterization of a new metallo- β -lactamase gene, *bla*_{NDM-1}, and a novel erythromycin esterase gene carried on a unique genetic structure in *Klebsiella pneumoniae* sequence type 14 from India. *Antimicrob Agents Chemother* 2009;**53**:5046–54.
- Groundwater PW, Xu S, Lai F, Varadi L, Tan J, Perry JD, et al. New Delhi metallo- β -lactamase-1: structure, inhibitors and detection of producers. *Future Med Chem* 2016;**8**:993–1012.
- Khan AU, Maryam L, Zarrilli R. Structure, genetics and worldwide spread of New Delhi metallo- β -lactamase (NDM): a threat to public health. *BMC Microbiol* 2017;**17**:101.
- King DT, Worrall LJ, Gruninger R, Strynadka NC. New Delhi metallo- β -lactamase: structural insights into β -lactam recognition and inhibition. *J Am Chem Soc* 2012;**134**:11362–5.
- Linciano P, Cendron L, Gianquinto E, Spyrikis F, Tondi D. Ten years with New Delhi metallo- β -lactamase-1 (NDM-1): from structural insights to inhibitor Design. *ACS Infect Dis* 2019;**5**:9–34.
- Song G, Wang W, Li Z, Wang Y, Wang J. First identification of isatin- β -thiosemicarbazones as novel inhibitors of New Delhi metallo- β -lactamase-1: chemical synthesis, biological evaluation and molecular simulation. *Chin Chem Lett* 2018;**29**:899–902.
- Schnaars C, Kildahl-Andersen G, Prandina A, Popal R, Radix S, Le Borgne M, et al. Synthesis and preclinical evaluation of TPA-based Zinc chelators as metallo- β -lactamase inhibitors. *ACS Infect Dis* 2018;**4**:1407–22.
- Ma J, Cao Q, McLeod SM, Ferguson K, Gao N, Breeze AL, et al. Target-based whole-cell screening by ¹H NMR spectroscopy. *Angew Chem Int Ed Engl* 2015;**54**:4764–7.
- King AM, Reid-Yu SA, Wang W, King DT, De Pascale G, Strynadka NC, et al. Aspergillomarasmine A overcomes metallo- β -lactamase antibiotic resistance. *Nature* 2014;**510**:503–6.
- Liu Z, Li J, Wang X, Liu D, Ke Y, Wang Y, et al. Novel variant of New Delhi metallo- β -lactamase, NDM-20, in *Escherichia coli*. *Front Microbiol* 2018;**9**:248.
- Khan A, Faheem M, Danishuddin M, Khan AU. Evaluation of inhibitory action of novel non β -lactam inhibitor against *Klebsiella pneumoniae* carbapenemase (KPC-2). *PLoS One* 2014;**9**:e108246.
- Rahman M, Shukla SK, Prasad KN, Ovejero CM, Pati BK, Tripathi A, et al. Prevalence and molecular characterisation of New Delhi metallo- β -lactamases NDM-1, NDM-5, NDM-6 and NDM-7 in multidrug-resistant Enterobacteriaceae from India. *Int J Antimicrob Agents* 2014;**44**:30–7.
- Khan AU, Nordmann P. Spread of carbapenemase NDM-1 producers: the situation in India and what may be proposed. *Scand J Infect Dis* 2012;**44**:531–5.
- Siwek A, Stefanska J, Dzitko K, Ruszczak A. Antifungal effect of 4-arylthiosemicarbazides against *Candida* species. Search for molecular basis of antifungal activity of thiosemicarbazide derivatives. *J Mol Model* 2012;**18**:4159–70.
- Barcelos RP, Portella RL, Da RE, Fonseca AS, Bresolin L, Carratu V, et al. Thiosemicarbazone derivate protects from AAPH and Cu²⁺-induced LDL oxidation. *Life Sci* 2011;**89**:20–8.
- Kowol CR, Trondl R, Arion VB, Jakupec MA, Lichtscheidl I, Keppler BK. Fluorescence properties and cellular distribution of the investigational anticancer drug triapine (3-aminopyridine-2-carboxaldehyde thiosemicarbazone) and its zinc(II) complex. *Dalton Trans* 2010;**39**:704–6.
- Pandeya SN, Sriram D, Nath G, de Clercq E. Synthesis, antibacterial, antifungal and anti-HIV activities of Schiff and Mannich bases derived from isatin derivatives and N-[4-(4'-chlorophenyl)thiazol-2-yl] thiosemicarbazide. *Eur J Pharmaceut Sci* 1999;**9**:25–31.
- Heffeter P, Pape V, Enyedy EA, Keppler BK, Szakacs G, Kowol CR. Anticancer thiosemicarbazones: chemical properties, interaction with iron metabolism, and resistance development. *Antioxidants Redox Signal* 2019;**30**:1062–82.
- Ozerkan D, Ertik O, Kaya B, Kuruca SE, Yanardag R, Ulkuseven B. Novel palladium(II) complexes with tetradentate thiosemicarbazones. Synthesis, characterization, *in vitro* cytotoxicity and xanthine oxidase inhibition. *Invest N Drugs* 2019;**37**:1187–97.
- Kunos CA, Andrews SJ, Moore KN, Chon HS, Ivy SP. Randomized phase II trial of triapine-cisplatin-radiotherapy for locally advanced stage uterine cervix or vaginal cancers. *Front Oncol* 2019;**9**:1067.
- Chen G, Niu C, Yi J, Sun L, Cao H, Fang Y, et al. Novel triapine derivative induces copper-dependent cell death in hematopoietic cancers. *J Med Chem* 2019;**62**:3107–21.
- Dai L, Chen J, Cao Y, Del VL, Qin Z. Ribonucleotide reductase inhibitor 3-AP induces oncogenic virus infected cell death and represses tumor growth. *J Canc* 2018;**9**:4503–9.
- Xu Y, Zeng M, Yu D, Ren J, Li F, Zheng A, et al. *In vitro* assessment of the role of DpC in the treatment of head and neck squamous cell carcinoma. *Oncol Lett* 2018;**15**:7999–8004.
- Lovejoy DB, Sharp DM, Seebacher N, Obeidy P, Prichard T, Stefani C, et al. Novel second-generation di-2-pyridylketone thiosemicarbazones show synergism with standard chemotherapeutics and demonstrate potent activity against lung cancer xenografts after oral and intravenous administration *in vivo*. *J Med Chem* 2012;**55**:7230–44.
- He Z, Qiao H, Yang F, Zhou W, Gong Y, Zhang X, et al. Novel thiosemicarbazone derivatives containing indole fragment as potent and selective anticancer agent. *Eur J Med Chem* 2019;**184**:111764.
- Hu B, Wang B, Zhao B, Guo Q, Li ZH, Zhang XH, et al. Thiosemicarbazone-based selective proliferation inactivators inhibit gastric cancer cell growth, invasion, and migration. *Med Chem Comm* 2017;**8**:2173–80.
- de Oliveira JF, Lima TS, Vendramini-Costa DB, de Lacerda PS, Lafayette EA, Da SR, et al. Thiosemicarbazones and 4-thiazolidinones indole-based derivatives: synthesis, evaluation of antiproliferative activity, cell death mechanisms and topoisomerase inhibition assay. *Eur J Med Chem* 2017;**136**:305–14.
- de Oliveira JF, Da SA, Vendramini-Costa DB, Da CAC, Campos JF, Ribeiro AG, et al. Synthesis of thiophene-thiosemicarbazone derivatives and evaluation of their *in vitro* and *in vivo* antitumor activities. *Eur J Med Chem* 2015;**104**:148–56.
- Buckley LM, McEwan NA, Nuttall T. Tris-EDTA significantly enhances antibiotic efficacy against multidrug-resistant *Pseudomonas aeruginosa* *in vitro*. *Vet Dermatol* 2013;**24**:122–519.

37. Lambert RJ, Hanlon GW, Denyer SP. The synergistic effect of EDTA/antimicrobial combinations on *Pseudomonas aeruginosa*. *J Appl Microbiol* 2004;**96**:244–53.
38. Hayakawa K, Guo L, Terentyeva EA, Li X, Kimura H, Hirano M, et al. Determination of specific activities and kinetic constants of biotinidase and lipoamidase in LEW rat and *Lactobacillus casei* (Shir-ota). *J Chromatogr B* 2006;**844**:240–50.
39. Lineweaver H, Burk D. The determination of enzyme dissociation constants. *J Am Chem Soc* 1934;**56**:658–66.
40. Xu Y, Wang S, Hu Q, Gao S, Ma X, Zhang W, et al. CavityPlus: a web server for protein cavity detection with pharmacophore modelling, allosteric site identification and covalent ligand binding ability prediction. *Nucleic Acids Res* 2018;**46**:W374–9.
41. Ma X, Meng H, Lai L. Motions of allosteric and orthosteric ligand-binding sites in proteins are highly correlated. *J Chem Inf Model* 2016;**56**:1725–33.
42. Yuan Y, Pei J, Lai L. Binding site detection and druggability prediction of protein targets for structure-based drug design. *Curr Pharmaceut Des* 2013;**19**:2326–33.
43. Feng H, Liu X, Wang S, Fleming J, Wang DC, Liu W. The mechanism of NDM-1-catalyzed carbapenem hydrolysis is distinct from that of penicillin or cephalosporin hydrolysis. *Nat Commun* 2017;**8**:2242.
44. Shi X, Wang M, Huang S, Han J, Chu W, Xiao C, et al. H2depda: an acyclic adjuvant potentiates meropenem activity *in vitro* against metallo- β -lactamase-producing enterobacteriales. *Eur J Med Chem* 2019;**167**:367–76.